



Optimal waste heat recovery through humidification in 2-spool micro gas turbines: A comparative study of advanced humidified cycles

Aggelos Gaitanis^{a,b}, Francesco Contino^b, Ward De Paepe^a

^a Thermal Engineering and Combustion Unit, University of Mons (UMONS), rue de l'Épargne 56, Mons, 7000, Hainaut, Belgium

^b Institute of Mechanics, Materials and Civil Engineering (iMMC), Université catholique de Louvain (UCLouvain), Place du Levant, 2, Louvain-la-Neuve, 1348, Walloon Brabant, Belgium

ARTICLE INFO

Keywords:

2-spool micro gas turbine
Humidification
Waste heat recovery
HAT
mHAT
REVAP[®]

ABSTRACT

Incorporating water into a micro Gas Turbine (mGT) has proven effective in recovering waste heat, significantly enhancing electrical efficiency. Techniques such as steam injection, preheated water addition, and the use of a saturator in the Humid Air Turbine (HAT) concept show great potential for waste heat recovery. However, these methods have not been applied in 2-spool small-scale gas turbine systems. This study proposes a systematic approach to optimize 2-spool advanced humidified mGT cycles for heat recovery. A two-step method was used, starting with a black-box model to determine thermodynamic limits, achieving an 8.3% absolute efficiency increase by injecting 400 g/s of water. Several advanced humidified cycles were analyzed. The REVAP[®] cycle, identified as optimal, reduced stack temperature to 49.6 °C, achieving a 4.1% efficiency increase and an 11.2% reduction in fuel consumption. Despite its complexity, REVAP[®] outperformed cycles with saturation towers (HAT and mHAT) by maximizing heat recovery. HAT achieved the highest water injection with a 4% efficiency gain. However, none of the advanced simulated cycles reached the theoretical exergetic limit. This highlights the importance of cycle layout and design, especially under constraints like the number of heat exchanger units and water phase change dynamics.

1. Introduction

Research focused on improving gas turbine (GT) performance has long aimed at recovering heat from exhaust gases. Exploration of various cycle configurations, such as combined, evaporation, steam injection, gas/gas recuperation, and chemical recuperation cycles, suggests that combined cycles would likely remain dominant for large-scale production [1]. However, the mechanical complexity of these cycles and increased cost might limit their use in small-scale operations, where alternative configurations could be more suitable [2].

Incorporating mixed air/water working fluids in GTs can greatly enhance electrical efficiency, specific power output, and reduce NO_x emissions [3,4]. Literature identifies three main types of humidified systems for all GTs that are depicted in Fig. 1. This figure shows the humidification types specifically in two-stage machines [3–5]:

- GTs with fully evaporative water injection (Fig. 1(a)),
- GTs with steam injection (Fig. 1(b)),
- GTs with water injection through a saturator with a water recovery loop (Fig. 1(c)).

Numerous studies have investigated fully-evaporated water injection configurations in GTs (Fig. 1(a)). Alhazmy and Najjar showed that cooling inlet air with a spray can boost GT power by 1%–7% and efficiency by 3% [6]. Over-spray systems can enhance power output by 11%–21%, increase efficiency by 1.6%–4%, and reduce NO_x emissions by 21–41% [7]. Approximately 600 power plants have implemented spray intake air-cooling systems [8]. Roumeliotis and Mathioudakis explored water injection at different GT cycle points [9], while Wang et al. [10] and Ingistov et al. [11] studied water injection between compressor stages, finding it boosts power output. Wet compression, which injects water into the compressor to cool the air, improves overall GT performance but may increase wear and corrosion [12,13].

Steam injection (Fig. 1(b)) studies show advantages like a 45% power increase and a 10% efficiency gain [14]. Nishida et al. noted that regenerative steam injection improves thermal efficiency by recovering exergy from exhaust gases [15], while Traverso and Massardo highlighted its competitiveness for sub-10 MW_e sizes [16]. However, steam injection has a smaller impact on efficiency compared to water injection, as there is significant exergy destruction in the Heat Recovery Steam Generator (HRSG) component [17].

* Corresponding author at: Thermal Engineering and Combustion Unit, University of Mons (UMONS), rue de l'Épargne 56, Mons, 7000, Hainaut, Belgium.
E-mail address: AngelosEvripidis.GAITANIS@umons.ac.be (A. Gaitanis).

Symbols**Acronyms**

AC	Aftercooler
CC	Combustion Chamber
CHP	Combined Heat and Power
ECO	Economizer
HAT	Humid Air Turbine
HPC	High Pressure Compressor
HPT	High Pressure Turbine
IC	Intercooler
LPC	Low Pressure Compressor
LPT	Low Pressure Turbine
mGT	micro Gas Turbine
mHAT	micro Humid Air Turbine
REC	Recuperator
REVAP	REgenerative EVAPoration
SM	Surge Margin, %
STIG	Steam-Injected Gas Turbine
TIT	Turbine Inlet Temperature
TOT	Turbine Outlet Temperature
WI	Water Injection

Roman symbols

h	Specific enthalpy, J kg^{-1}
K_c	Choke constant, -
k	Heat capacity ratio
\dot{m}	Mass flow rate, kg s^{-1}
N	Rotational speed, rpm
P	Power, kW
p	Pressure, Pa
\dot{Q}	Heat flux, kW
T	Temperature, $^{\circ}\text{C}$
\dot{X}	Exergy flow, kW
x	Specific exergy, J kg^{-1}

Greek symbols

η	Efficiency, %
π	Pressure ratio, -

Subscripts

BB	Black Box
el	Electrical
ex	Exergy
in	Inlet
is	ISENTROPIC
out	Outlet
ref	Reference
sat	Saturated
th	Thermal
v	Vapor

Humid Air turbines (HAT) cycles (Fig. 1(c)), where water is injected into a humidification tower, show superior efficiency and specific power [18,19]. Kim et al. found higher ambient temperatures increase HAT cycle's specific work [20], and optimizations by Lazzaretto and Segato focused on minimizing compressed air temperature and maximizing heat use [21,22].

More sophisticated humidification techniques, such as the Advanced Humid Air Turbine (AHAT) [23], the Cascaded Humidified Advanced Turbine (CHAT) [24], TOP Humid Air Turbine (TOPHAT[®]) [25] and the REgenerative EVAPoration (REVAP[®]) [26] have been developed to address specific GT humidification issues or enhance performance. The AHAT cycle combines the HAT concept with inlet air cooling, using water atomization. Hitachi developed a 3 MW-class pilot plant for the AHAT system. Their tests showed significant improvements in electrical output and efficiency, validating the potential of AHAT technology for practical applications [27]. The CHAT cycle mitigates flow mismatch between the compressor and turbine [24], while the TOPHAT[®] cycle reduces compressor work by using hot water for spray compression between compressor stages [25]. Despite the high potential of these cycles, no commercial success has been presented.

Humidifying a GT cycle not only improves performance but also affects the surge margin, combustion stability, and water quality requirements [4]. Increased mass flow can reduce the compressor surge margin, potentially causing surge issues [28]. Water injection impacts combustion efficiency and stability, leading to increased CO emissions [5]. Different methods of water introduction require varying water quality levels, influencing energy costs.

Similarly, mGT (2–400 kW_e) humidification follows three areas as in large-scale GTs (1–100 MW_e): liquid water injection, steam injection, and water injection in a saturator with a recovery loop. The main difference in mGTs is the presence of a recuperator (REC) and single-stage compression/expansion in most cycles.

Injecting liquid water (Fig. 1(a)) before the compressor, through methods like inlet air cooling or wet compression, lowers the compressor inlet temperature. Brandon et al. reported power increases from 57 to 70 kW_e with evaporative cooling at 33 $^{\circ}\text{C}$ ambient temperature [29]. Dodo et al. and Nakano et al. showed a 6 kW_e increase in a 150 kW_e mGT with WAC [30]. Renzi et al. demonstrated 5% to 13% power gains with inlet fogging on a T100 mGT, with 0.41% efficiency improvement per degree Celsius [31]. Preheated water injection at the recuperator inlet for evaporative aftercooling lowers compressed air temperature, improving heat recovery. De Paepe et al. found this optimal for waste heat recovery in a Turbec T100 [32], showing efficiency and power gains lower than steam injection when limited to 100% relative humidity [33]. Zhang and Xiao reported power increase from 82.5 to 106.2 kW_e and a 3.05% efficiency gain [34]. Water injection into the combustor reduces combustion temperatures and NO_x, offering limited benefits for mGTs with already low NO_x emissions [2]. Lee et al. showed power increase from 22.6 to 29.7 kW_e but a 23.4% efficiency drop in a 30 kW_e mGT [35].

Steam injection (Fig. 1(b)), post-compression, improves efficiency using exhaust heat to auto-raise steam. Lee et al. found an 8.6% efficiency gain with steam injection pre-recuperator [35]. Mochizuki et al. reported 3%–4% efficiency gains and reduced NO_x in a Capstone C60 [36]. Ferrari et al. and De Paepe et al. confirmed stable operation and increased efficiency of the T100 mGT [37,38].

Water injection using a saturation tower (Fig. 1(c)), converting mGTs to mHAT or mHAT+ cycles, offers the highest efficiency gains. Rao's HAT concept, applied to mGTs by Parente et al. showed 3%–5% efficiency and 50%–70% specific work gains [39]. De Paepe et al. demonstrated efficiency increase from 30 to 33% with a saturation tower on a Turbec T100 [28]. Shandong University developed a saturator for an 80 kW mGT, optimizing humidification for better performance [40]. mHAT and mHAT+ cycles provide the highest performance improvements, with simple layout and lower costs. Economic analyses show significant savings, making them suitable for distributed CHP generation [41]. However, despite a 3% efficiency increase, mHATs are not yet financially viable under current cogeneration policies [42]. More complex cycles like AHAT and REVAP[®], although more efficient, face adoption challenges due to higher costs and complexity [17,43].

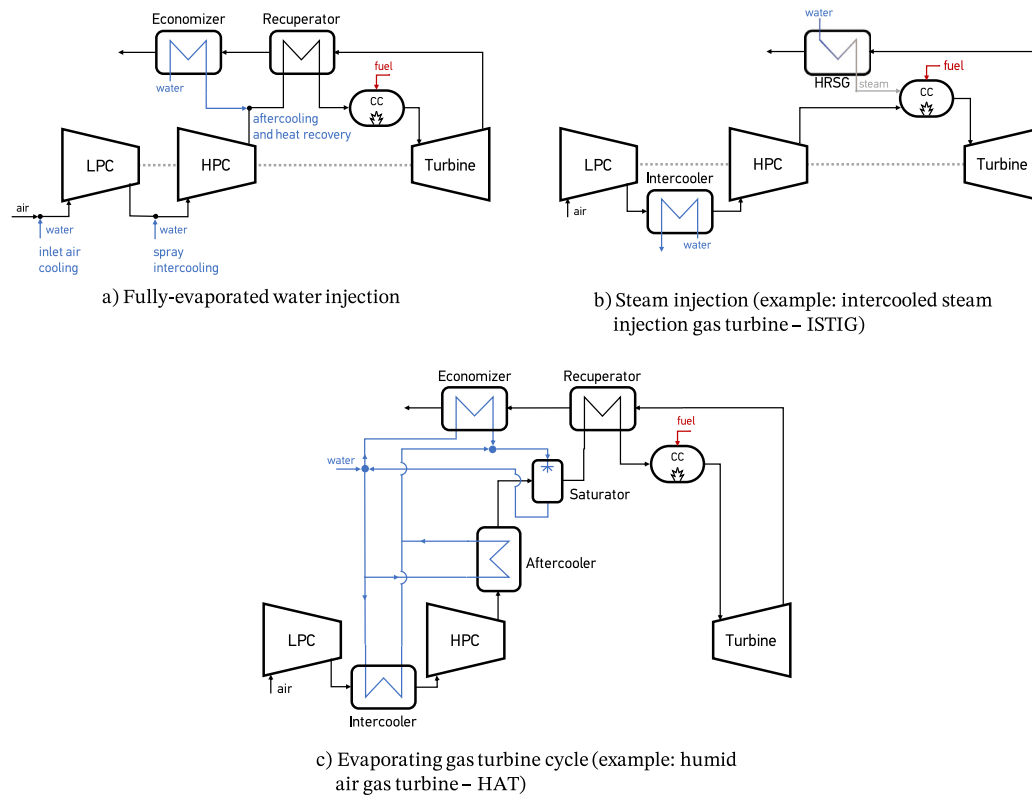


Fig. 1. A layout of the 3 possible different humidification techniques in 2-spool GT cycles. (a) Shows the injection of water that is fully evaporated in 3 possible locations in the cycle. (b) Presents a steam injection example in an intercooled GT and (c) presents an evaporative GT cycle with the use of saturation tower.

While this article focuses on humidification-based waste heat recovery, other promising strategies exist in the literature. Thermochemical recuperation (TCR), particularly through steam methane reforming (SMR), offers an efficient pathway for exhaust heat utilization. Pashchenko et al. [44–46] have explored chemically recuperated gas turbines, showing that TCR can significantly enhance efficiency and hydrogen production by recovering heat directly through endothermic reactions. SMR shows higher gas turbine efficiency than steam injected GT especially at turbine inlet temperature (TIT) above 1000 °C [44]. However, this method is typically less suited for mGTs which operate at lower TIT due to the absence of turbine cooling. Moreover, a two-step analysis using black box and heat exchanger network has been used to find the optimal natural gas steam reforming concept in combined cycle with external and internal firing of biomass [47].

This study presents an analysis aimed at identifying the most effective method for waste heat recovery through water introduction in 2-spool mGTs. Although numerous studies focused on humidification in conventional recuperated mGTs a research gap remains regarding a comprehensive analysis to identify the optimal approach for waste heat recovery in two-shaft microturbines. The inclusion of heat exchangers after each compression stage in 2-spool mGT allows us to utilize them in the waste heat recovery process and investigate further the potential of humidification. We employed a two-step simulation process to ascertain the optimal waste heat recovery in configurations with water injection. The study is divided in four main sections. The modeling approaches of the two-step analysis are presented in the “Methodology” section. The thermodynamic limit with water injection is determined with a black-box approach, as detailed within “Black box analysis” section. Subsequently, we assessed and compared advanced humidified mGT concepts in the “Advanced humidified cycles” section. We designed several possible cycle layouts utilizing composite curve theory. Simple concepts, like direct water injection layout, and more complex ones (mHAT, HAT, REVAP[®]) are compared. Also the cycles

are tested if they can reach the thermodynamic limit which is established in the “Black box analysis” section. So the cycles are assessed based on their performance and complexity. Finally the “Conclusions” section demonstrates all the main outcomes and findings of the two-step analysis along with the takeaway messages and future perspectives.

2. Methodology

To eliminate the reliance on guesswork for identifying the most efficient configuration for heat recuperation of an advanced humidified 2-spool mGT cycle, a structured methodology is employed. This approach starts with a two-step method aimed at identifying the most effective cycle arrangement. First, the maximum thermodynamic potential is set using an abstract model for the heat exchangers in combination with second-law analysis, as described in Section 3. More specifically, in this phase, a black box model substitutes the heat exchanger network allowing both the first and second laws of thermodynamics to be applied. Optimal thermodynamic performance is achieved by capping the maximum exergetic efficiency at 93% and minimizing exergy destruction to 5%, following the guidelines of El-Masri [48]. The next step involves determining the cycle layout that meets this optimal performance by defining various heat exchanger network configurations in Section 4. Each network’s feasibility is then assessed using composite curve theory and pinch analysis.

The modeling of the water injection cycle using black box and then the various advanced humidified mGT cycles is conducted with the simulation model that is developed by the authors of this article [49]. This model simulates the steady-state operation of a 2-spool mGT which has the same operating characteristics as the Aurelia A400 machine [50]. Moreover this model was compared against data from Aurelia A400 that were found in literature. For the turbomachinery components, the compressor maps are adopted from Jaatinen-Värrä et al. [51]. The isentropic efficiency of low and high pressure turbines (HPT, LPT) is 84% and both components are considered to be choked. As a substantial

amount of water is introduced in the cycle, the choking condition is adjusted by altering the turbine's choking constant to account for changes in the turbine inlet gas composition, as outlined in [52]:

$$K_c = \frac{\dot{m}_T \sqrt{TIT}}{p_{in,T}} = A \sqrt{\frac{k_T}{R} \left(\frac{2}{k_T + 1} \right)^{\frac{k_T+1}{k_T-1}}}, \quad (1)$$

where A is the cross-sectional area of the turbine, $p_{in,T}$ is the inlet pressure, k_T is the mean heat capacity ratio of the gas, R corresponds to the gas constant and TIT refers to the Turbine Inlet Temperature. A is determined for LPT and HPT using the design steady state point of literature data [51]. Moreover the isentropic efficiency is corrected with as suggested by Parente et al. [53]:

$$\frac{\eta_{is}}{\eta_{is}^*} = \frac{k-1}{k^*-1} \sqrt{\frac{k^*+1}{k+1} \frac{1-1/\pi^{(k^*-1)/k^*}}{1-1/\pi^{(k-1)/k}}}, \quad (2)$$

where the properties of standard dry air are presented with an asterisk (*) and π is the pressure ratio of the component.

The combustion chamber (CC) of the engine is assumed to remain unchanged, operating with a combustion efficiency of 99% [54]. The reaction is modeled using the optimized GRI-Mech 3.0 mechanism, specifically designed for natural gas combustion [55]. This analysis does not account for potential combustion instabilities, as the water fraction in the gas, even at the maximum injection rate (18% as per the black box water injection limit), stays below the 30% threshold [56] at which CO levels would impact the stability of premixed combustion. A mixture of 91.2% vol. methane, 6.7% vol. ethane and 2.1% vol. propane is chosen for the fuel same as in previous study [49]. The pressure loss in this component is 3%.

2.1. Mixing model

For the determination of the thermodynamic values of the fluid properties the Coolprop library [57] is used. However, for the purposes of this analysis, air is mixed with water and condensation can occur. Also the water content in the flue gasses can condense due to increased waste heat recovery. Therefore an algorithm is created to determine the liquid water due to condensation in a mixture. The condensation algorithm is presented in Fig. 2. First of all an initial temperature $T_{out} = T_{mix}$ is calculated using the energy balance of water and air mixing and/or with energy extraction according to

$$(\dot{m}_{gas,in} + \dot{m}_{water,in})h_{out} = \dot{m}_{gas,in}h_{gas,in} + \dot{m}_{water,in}h_{water,in} - \dot{Q}, \quad (3)$$

where $\dot{m}_{gas,in}$ and $\dot{m}_{water,in}$ represent the mass flow rates of air/gas and water, respectively. The terms $h_{gas,in}$ and $h_{water,in}$ refer to the specific enthalpies of the air/gas and water, while \dot{Q} denotes the energy extraction (such as in the case of a heat exchanger). After the calculation of h_{out} , a root-finding algorithm fsolve [58] determines the T_{mix} assuming the enthalpy is in gas phase. This initial temperature is used to calculate the initial saturation pressure of water p_{sat} . The partial pressure of water in the mixture is calculated as

$$p_{H_2O} = p_{out} y_{H_2O}, \quad (4)$$

where y_{H_2O} is the proportion of moles of water relative to the total moles present in the mixture. If $p_{H_2O} \geq p_{sat}$ the model enters the condensation loop that is shown in Fig. 2 dotted box. Inside the loop, a mass fraction for the vapor water content of the mixture (x_v) is indicated and the energy balance of the two-phase mix is calculated as

$$h_{gas,mix} = \frac{h_{gas,in}/(1+x_{w/a}) + x_{w/a}h_{water,in}/(1+x_{w/a}) - q - (x_{H_2O} - x_v)h_1}{1 - x_{H_2O} + x_v}, \quad (5)$$

where $h_{gas,mix}$ is the specific mixture enthalpy in gas phase, h_1 is the liquid water enthalpy, x_{H_2O} is the mass fraction of water in the mixture,

Table 1
Input parameters for the comparison of mixing model.

		1	2	3
$T_{water,in}$	[°C]	54.2	57.3	62.1
$p_{water,in}$	[bar]	3.92	3.92	3.92
\dot{m}_{water}	[g/s]	84	131	155
$T_{air,in}$	[°C]	103.9	109.25	110.2
$p_{air,in}$	[bar]	2.97	3.6	3.92
\dot{m}_{air}	[kg/s]	1.16	1.36	1.61

x_v is the mass fraction of water vapor in the mixture, $x_{w/a}$ is the ratio of mass of water injected divided by the mass of gas at the inlet ($\dot{m}_{water,in}/\dot{m}_{gas,in}$), q is the energy extraction divided by the mass flow rate of the mixture. So this iterative process (presented in Fig. 2) calculates the enthalpy of the gas and liquid phase of the mixture, the temperature and the liquid mass fraction. The enthalpy (h) calculation and all energy related values (entropy, internal energy) in the study are subtracted by the reference state such as $h = h_{CP} - h_{CP,ref}$, where h_{CP} is the specific enthalpy calculated by Coolprop at the state of interest and $h_{CP,ref}$ is the specific enthalpy at the reference state of 15 °C, 1 bar. By using a reference state, the impact of the chosen zero point is eliminated and the study focuses on the meaningful changes in energy as Coolprop uses different zero points for each property.

Even though this model applies the validated Coolprop pure fluid thermophysical library [57], the performance of mixing model is also compared against other known thermodynamic properties libraries. Thus three different points of air and water mixing calculated from the mixing model are compared with the UNIFAC library [59] and REFPROP library [60]. The values were chosen to be in range with black box analysis. The mixing temperature is calculated with these libraries in three inlet temperatures, pressures and mass flow rates of air and water (see Table 1) using UNIFAC and REFPROP from Aspen Plus® [61].

Fig. 3 shows the mixture temperature relative error of the mixing model against UNIFAC and REFPROP in three different air mass flow rates. The temperature difference of the model against other thermophysical libraries is very small. The maximum absolute error is 0.12% and is calculated at point 3 (see Table 1). The root mean squared error (RMSE) for REFPROP and UNIFAC is 0.0497 and 0.076 respectively. Therefore the validity of our method is confirmed.

2.2. Saturator model

During the research for the most effective humidified 2-spool mGT configuration, different cycles that employ a saturation tower are studied. Therefore the modeling method of the saturator should be presented.

Many humid air turbine systems employ a packed-bed humidification tower [4]. The tower features a casing that holds surface area-enhancing materials or packing, along with components such as a water distributor, collector, support grids, and a droplet eliminator. Given that humidification in mGT cycles occurs at elevated temperatures, the packing materials are constructed from stainless steel. Within the saturation tower, air ascends and interacts with a counter-flow of hot water. This process heats and humidifies the air, bringing it to a specific final temperature and humidity level, which are determined by the operating pressure and the inlet temperatures of both the water and the air. In the current study the saturator performance is not assessed on a case-by-case model but design conditions are applied in this component. Thus, we use a generic approach and assume an idealized but realistic saturation tower.

Considering the saturator as a simple control volume, the mass balance equations are as follows

$$\dot{m}_{air,out} = \dot{m}_{air,in} + \dot{m}_{sat}, \quad (6)$$

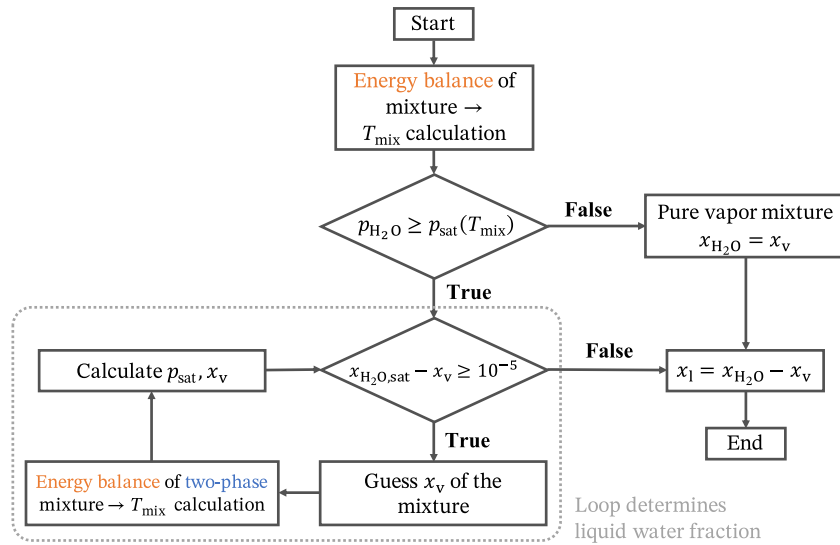


Fig. 2. The liquid mass fraction the mixture temperature and the specific enthalpies of the gas and liquid phases are determined through an iterative algorithm.

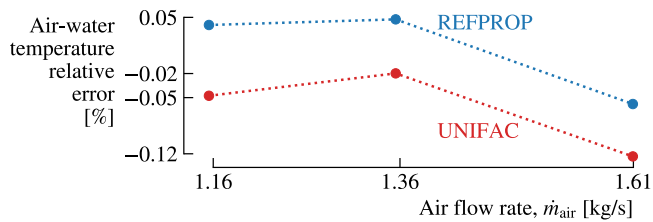


Fig. 3. The mixing temperature error is below 0.2% with maximum absolute error of 0.12% against the UNIFAC library.

$$\dot{m}_{\text{sat}} = \dot{m}_{\text{water,out}} - \dot{m}_{\text{water,in}} \quad (7)$$

\dot{m}_{sat} is the mass flow rate of water that is evaporated and mixed with the air flow. The energy balance can be expressed as

$$(\dot{m}_{\text{air,in}} + \dot{m}_{\text{sat}})h_{\text{mix,out}} = \dot{m}_{\text{air,in}}h_{\text{air,in}} + \dot{m}_{\text{water,in}}h_{\text{water,in}} - (\dot{m}_{\text{water,in}} - \dot{m}_{\text{sat}})h_{\text{water,out}} \quad (8)$$

The water outlet temperature is assumed to be 5 °C higher than wet-bulb temperature (adiabatic saturation temperature) so $T_{\text{water,out}} = T_{\text{wet-bulb}} + 5$ [62]. Using wet-bulb temperature instead of dry bulb temperature is necessary because it provides a comprehensive measure of the air's thermal and moisture content, essential for accurately modeling the humidification process in the saturation tower. The wet-bulb temperature ensures that the energy balance and system efficiency calculations reflect both sensible and latent heat transfers, leading to more accurate and realistic simulation.

3. Black box analysis

In the first step of the two-step design approach, all heat exchangers in the 2-spool mGT layout were removed and replaced with a single black box, as depicted in Fig. 4. This adiabatic black box serves as the heat recovery unit for the cycle. Following this, a network of generic heaters and coolers functioning as a black box system is proposed, as recommended in the literature [26,33]. The black box network method described in the literature for intercooled evaporated cycles has been slightly modified to include two turbine and generator components [26], which is then employed for the simulations in this study.

The intercooler of stage 2–3 in Fig. 4 of black box cools the air after the first compression stage of the LPC. Water is then introduced into the compressed air after it passes through the HPC. Before the air/water mixture enters the combustion chamber, it is preheated in the heater. The flue gases exiting the turbine are subsequently cooled in the cooler before being released through the stack. The conservation of energy within the black box allows us to express the relationship between the thermal energy flows exchanged by the intercooler, heater, and cooler as follows:

$$\dot{Q}_{\text{heater}} + \dot{Q}_{\text{cooler}} + \dot{Q}_{\text{intercooler}} = 0 \quad (9)$$

The boundary conditions and all the necessary parameters for the modeling of the 2-spool mGT with a black box heat recovery system are depicted in Table 2. The cycle is modeled using the two control parameters of a standard mGT cycle which are a constant Turbine Outlet Temperature (TOT) of 645 °C and a constant electrical power output of 400 kW_e [63]. The LP and HP rotational speeds are considered equal for 400 kW_e according to the operational characteristics of Aurelia A400 [49,51]. Although the 2-spool mGT is modeled with equal shaft speeds preliminary optimization studies indicate that adjusting the low- and high-pressure spool speeds can offer modest performance improvements of less than 0.5%. While this added efficiency is beneficial, it remains relatively small, confirming that the assumption of equal shaft speeds is reasonable for the purposes of this analysis. The temperature difference between the cold side outlet and the hot side inlet of the black box (hot pinch) is set at $\Delta T_{\text{hot}} = 50$ °C [17]. This temperature difference also ensures a 90% of effectiveness if the heater and cooler are substituted with a recuperator which is a design value for the Aurelia A400 [51]. The temperature in the outlet of intercooler is also set constant at $T_3 = 50$ °C to account for a realistic and conservative heat recovery after the LPC according to De Ruyck et al. [26] assuming that the cold side inlet temperature in the intercooler is 40 °C. Therefore the cold pinch of the intercooled is $\Delta T_{\text{cold, IC}} = 50 - 40 = 10$ °C. The pressure losses presented in Table 2 for the heat recovery system are taken from a study on the design of Aurelia A400 [64] after a consultation from manufacturers and thus are considered feasible. A third control parameter is chosen to solve the system of equations: the air-to-water ratio ($x_{w/a} = \dot{m}_{\text{water}}/\dot{m}_{\text{air}}$). This parameter is increased from 0 to 25% with a step of 1%. The stack temperature is determined by solving the Eq. (9) knowing the fluid properties and the hot pinch.

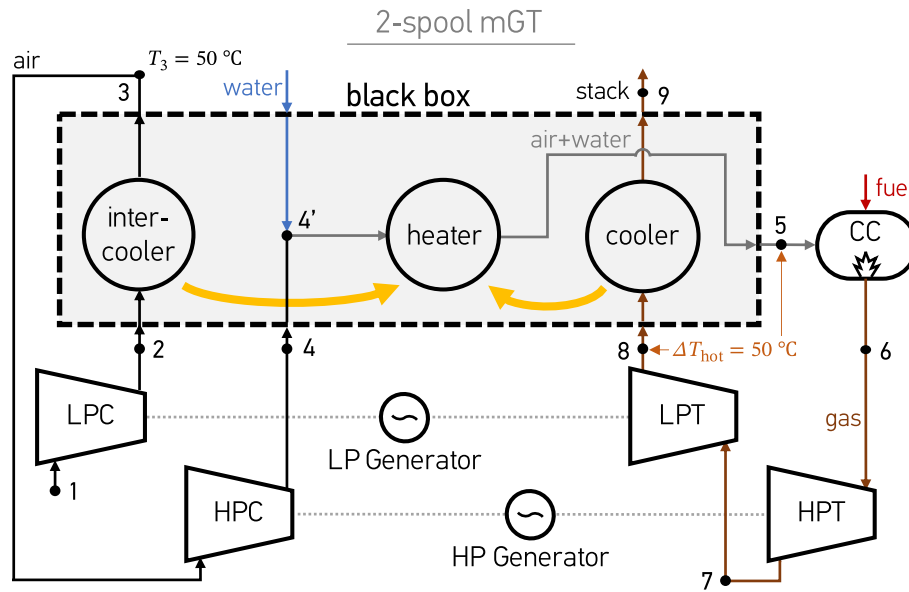


Fig. 4. The black box of the heat recovery system for the 2-spool mGT consists of an intercooler, heater and cooler. The air is injected at stage 4' in the HPC outlet.

Table 2
Boundary conditions for the simulation of the 2-spool mGT using a black box for the heat recovery system.

Low-pressure compressor - LPC		
Pressure ratio	Variable ^a	
Isentropic efficiency	Variable ^a	
Inlet air temperature	15 °C	
High-pressure compressor - HPC		
Pressure ratio	Variable ^a	
Isentropic efficiency	Variable ^a	
Inlet temperature	50 °C	
Combustion chamber		
Combustor pressure loss	3%	[64]
Combustion efficiency	99%	[54]
High-pressure turbine - HPT		
Isentropic efficiency	Variable ^b	
Low-pressure turbine - LPT		
Isentropic efficiency	Variable ^b	
Turbine Outlet Temperature (TOT)	645 °C	[65,66]
Heat recovery system - black box		
Cold side pressure loss	1%	[64]
Hot side pressure loss	3%	[64]
Water injection pressure loss	0.5%	[17]
Hot inlet/cold outlet temperature difference	50 °C	[17]
Injected water flow rate	Variable	
Feed water inlet temperature	15 °C	
Fuel		
Fuel temperature	30 °C	[33]
Fuel pressure	6 bar	[33]
Lower Heating Value	49.5 MJ/kg	[49]
Performance		
Electric power	400 kW _e	
LP and HP rotational speeds	$N_{LP} = N_{HP}$	[51]

^a Efficiency is determined from compressor maps [51].

^b The isentropic efficiency is a function of the gas properties according to Eq. (2).

3.1. Exergy analysis

The black box is assessed based on the exergy content of its streams in the cycle. Thus, exergy destruction, when divided by the total exergy input from the fuel, is defined as:

$$\eta_{\text{dest, BB}} = \frac{\sum_{\text{in}} \dot{X} - \sum_{\text{out}} \dot{X}}{\dot{X}_{\text{fuel}}}, \quad (10)$$

\dot{X}_{fuel} is the exergy input of the cycle presented as $x_{\text{fuel}} \dot{m}_{\text{fuel}}$. The chemical exergy of the fuel (x_{fuel}) represents the amount of energy that can be obtained through direct conversion at ambient temperature of chemical exergy into work without passing through a thermal state. In

this study, it is computed according to Balli et al. [67]:

$$\frac{x_{\text{fuel}}}{\text{LHV}} \approx 1.033 + 0.0169 \frac{b}{a} - \frac{0.0698}{a}, \quad (11)$$

where a, b refer to hydrocarbon fuels as $C_a H_b$. Consequently, for the fuel mixture considered in this study, $x_{\text{fuel}}/\text{LHV} = 1.0343$. Exergy efficiency of the black box is the sum of exergy gained by the streams divided by the sum of exergy lost by the streams, expressed as:

$$\eta_{\text{ex, BB}} = \frac{\sum_{\text{gain}} \Delta \dot{X}}{\sum_{\text{loss}} \Delta \dot{X}}. \quad (12)$$

Therefore, exergy efficiency is the ratio of the exergy gained by the air at the HPC outlet ($\dot{X}_5 - \dot{X}_4$) and the sum of the exergy loss in the LPC outlet ($\dot{X}_2 - \dot{X}_3$) and in the flue gases ($\dot{X}_8 - \dot{X}_9$). All the exergy flows are subtracted by the reference exergy (dead state) which is set at 15 °C and 1 bar. Also the ambient air is considered to be at dead state and has 60% humidity.

The simulation of the cycle occurs at every 1% step of the water-to-air ratio, so exergy destruction and efficiency are obtained at every step. According to the literature, the minimal total exergy destruction is 5% and the maximum black box exergy efficiency is 93% for large-scale GTs [33,48]. These values are established as limits for the heat transfer system. Surpassing these limits would lead to impractical designs that cannot be realized with actual heat exchangers.

Additionally, the compressor surge margin, a key metric for identifying potential flow instabilities in the component, is calculated as shown in Eq. (13):

$$SM = \frac{\dot{m}_c - \dot{m}_{c,sl}}{\dot{m}_c} \Big|_{N=\text{const}} \times 100\%, \quad (13)$$

where $\dot{m}_{c,sl}$ represents the mass flow rate at the surge line assuming constant rotational speed [68]. The surge line is defined as the boundary beyond which the compressor becomes aerodynamically unstable, leading to stall and strong pressure oscillations. As the compressor maps of this study are taken from CFD, the surge point for each speed line is identified by progressively decreasing the mass flow rate and observing when the compressor flow field shows signs of instability. According to Cumpsty it is identified as the last converged point in steady simulations [69]. This metric is used in the current study to identify operational limitations in the two compressors as water is injected.

3.2. Black box results

This section first addresses the operational issues that can occur by water injection. Secondly, significant parameters of the cycle are presented and discussed as the amount of water is increased. Then, the results of the exergy analysis of the black box are examined.

Water injection between the compressors and turbines causes a mass flow imbalance, increasing turbine power and electric output. To stabilize power, as water is increasing the shaft speeds are reduced which leads to a lower pressure ratio and air mass flow rate. This adjustment shifts the compressor's operation point towards the surge line. According to Walsh, a minimum surge margin of 15% is necessary for low-pressure compressors in power generation applications to avoid flow instabilities [70]. However, Walsh calculates the surge margin using a different formula ($SM = (\pi_{\text{surge}} - \pi_{\text{working line}}) / \pi_{\text{working line}} \times 100$) mainly for large-scale GTs. The calculation from De Paepe et al. [68] (Eq. (13)) is more appropriate for centrifugal compressors of mGTs as they have flatter iso-RPM lines near the surge line. Therefore applying the calculation of Eq. (13), a 10% of surge margin is sufficient and it is used as manufacturing limitation in the simulations [71].

Water injection can also cause combustion instability, reducing efficiency and increasing emissions. However, adding water lowers temperatures resulting in a significant reduction in NO_x emissions. It can also decrease flame speed and prevent flashback in hydrogen enriched fuels [72]. Condensed water from steam injection cycles contains ions and dissolved CO₂, requiring water treatment before recycling. Low-temperature water condensation creates acidic conditions, necessitating corrosion protection for heat exchangers and stacks [73]. Therefore the combustor inlet temperature should be assessed as water is introduced in the cycle to verify the flame stability in CC.

As you increase the injected water flow rate in the cycle, the water at stage 4' (see Fig. 4) it changes from fully evaporated to two-phase. However all possible liquid droplets in the stream are evaporated in the heater (4'-5) as the temperature at combustor inlet is fixed at 595 °C by both the constant TOT and the hot pinch. This verifies that potential

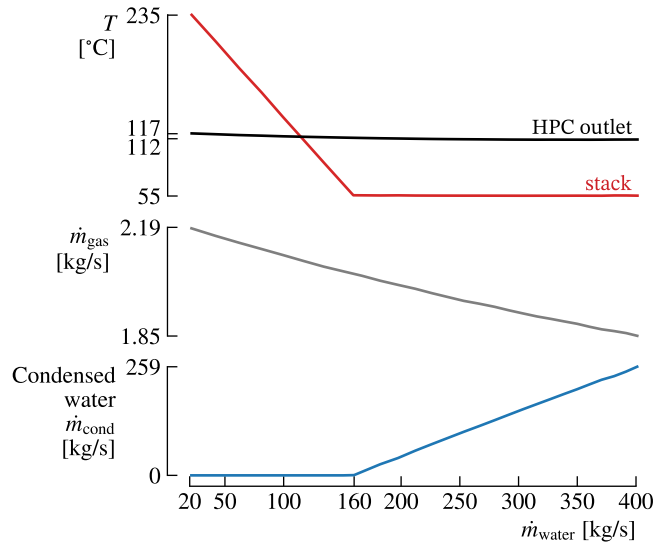


Fig. 5. The stack temperature decreases with an increasing amount of water and condensation in the flue gases occurs at 160 g/s. The mass flow rate of the cycle decrease with as the amount of injected water rises.

flame stability issues in the combustor are avoided and also liquid water particles are not entering the HPT. However using an actual heat exchanger with a fixed surface does not ensure this high combustor inlet temperature. Thus low CIT is avoided in that case by using larger heat exchanger components.

Fig. 5 shows the behavior of the stack temperature while the amount of water in the cycle rises. As the injected water flow rate increases, the stack temperature decreases almost linearly until 6% of water-to-air ratio ($\dot{m}_{\text{water}} = 160$ g/s). Increasing water injection requires greater heat exchange between the flue gases and the wet compressed air (point 4'). This increased heat exchange is the result of the fixed TOT together with the constant hot pinch temperature of 50 °C. As the temperature at point 8 is fixed, the low temperature at point 4' enhances the heat exchange. The reduction in stack temperature stagnates at 55 °C. At this point, the increasing need for heat addition at the heater cools the flue gases down below their dew point, releasing latent heat and preventing further temperature reduction and linearly increasing the condensed water in flue gases. The total amount of condensed water in the stack is also illustrated in Fig. 5. At 400 g/s of injected water, the condensed water flow rate has the same order of magnitude (259 g/s). Also the temperature decrease in the HPC outlet is very small (from 117 to 112 °C) as the water content increases. Fig. 5 shows the exhaust gas mass flow rate which decreases from 2.19 to 1.85 kg/s as the water reached 400 g/s.

The simulations were carried out until the operating point of the cycle reached the surge line of LPC. Fig. 6 shows the wet operating line in both compressors that is illustrated as the amount of water is increased and the electric power is kept constant. The surge line is reached at 0.5 kg/s of injected water (35% water-to-air ratio). So to keep a 10% surge margin the limit for water injection is 0.4 kg/s (28% water-to-air ratio). As it was mentioned in the description of the boundary conditions, the two shafts are set to have equal rotational speeds as this is the design assumption for nominal power. Also operational optimization is beyond the aim of this paper. Thus, the wet operating line of HPC shows that this component does not present any risk of surge as at the LPC's surge margin of 10%, HPC shows a surge margin of 25%. Also HPC's operating line shows a decrease in normalized mass flow rate because the inlet temperature is fixed at 50 °C (intercooler constraint), the shaft speed is equal with the LPC speed and the mass

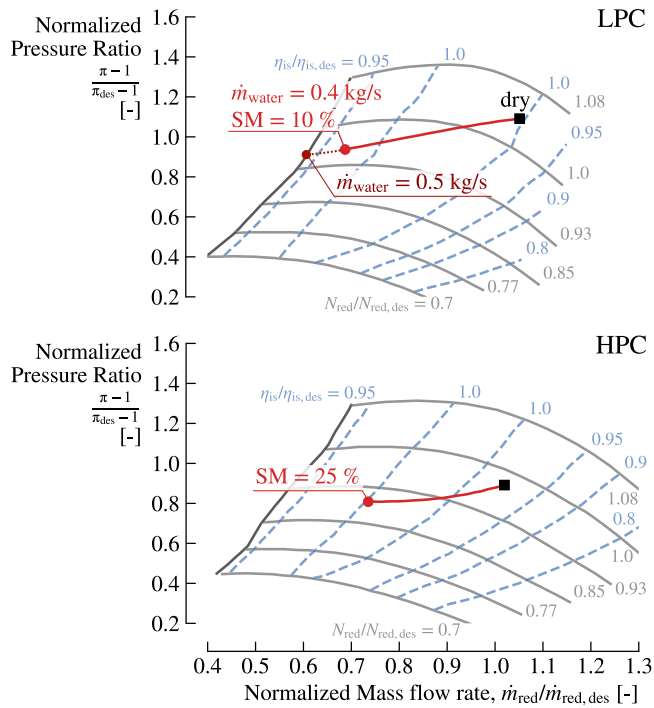


Fig. 6. The wet operating line for constant power at 400kW_e moves towards the surge line as the water injection increases. At 10% SM in the LPC the amount of water is 0.4kg/s and this the limit for the calculations.

the air flow rate decrease has a higher impact than the inlet pressure which also drops.

This reduction in pressure ratio and mass flow rate shifts the operating line closer to the surge line in both compressors. This behavior is associated with three key characteristics of the mGT:

- The turbines are choked so an increase in injected water should decrease the mass flow rate of air.
- A higher heat exchange allows the compressors to pressurize less the flow in order to achieve the same electric power.
- The increase of mass flows in the turbines utilizes more work and moves the operating point to lower air flow rate for the same power output.

The Black box exergy efficiency and destruction for several water-to-air ratios is depicted in Fig. 7. A decrease in black box exergy efficiency is observed until 6% of water fraction. Then the efficiency increases gradually and reached the 92% at the water injection limit. A reversed behavior is shown for the BB exergy destruction. This parameter increases in water ratios below 6% and reaches the maximum showing 10.8%. As the amount of water rises further, BB exergy destruction decreases to reach 7.9% at the water injection limit. Both values at 25% water-to-air ratio are within the acceptable limits from the literature, meaning that the heat recovery system (black box) can be realistically designed [33,48].

The behavior of the BB exergy efficiency and destruction is explained by presenting the exergy flows of inputs and outputs in the black box at Fig. 8. The exergy gain and losses in the different black box components are also depicted with double arrows. The exergy flow of the feedwater is not depicted as the water is introduced into the black box at atmospheric temperature and slightly pressurized (15 °C, 4.7 bar) and its impact in the exergy efficiency and destruction is minimal ($\dot{X}_w = 0.15$ kW at 28% of water-to-air ratio).

The specific behavior of the various exergy flows depicted in Fig. 8 is closely tied to the fundamental operating principles of the mGT.

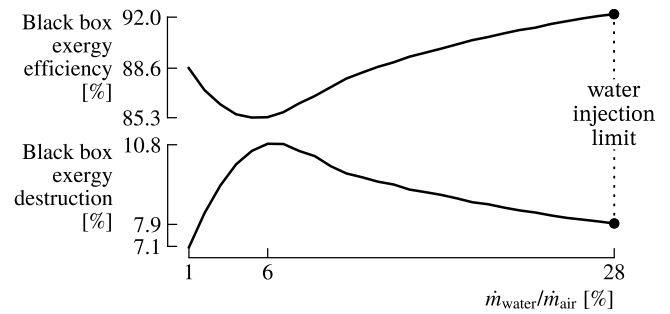


Fig. 7. Black box exergy efficiency and destruction show opposite behaviors as the amount of water increases. At 10% of LPC surge margin, BB exergy efficiency shows 92% which is lower than the literature limits [33,48].

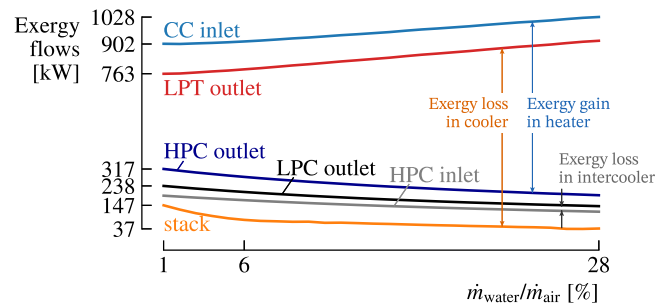


Fig. 8. The exergy fluxes, as the water injection mass flow rate increases, show a gradual decrease in the exergy losses compared to the exergy gain in the heater.

As water injection increases, the exergy flow through the HPT and LPT exhausts elevates due to the augmented water content in the flow. Since the TOT remains constant, a reduced TIT is necessary to achieve the same work output. The exergy flow at the combustor inlet remains fairly stable because the increase in exergy, attributed to the higher temperature and water content, is balanced by a reduction in pressure and mass flow rate, which results from the lower rotational speed governed by the mGT controller. The reduction in pressure ratio, mass flow rate, and compressor outlet temperature causes a decrease in the exergy flow entering the black box from the LPC and HPC outlets. Similarly, the exergy flow at the HPC inlet diminishes due to the decreased mass flow rate and pressure drop, while the temperature remains constant. With increased water injection, the stack temperature progressively decreases, thereby reducing the exergy flow exiting through the stack. From the point of 160 g/s (6% water ratio) of water injection onwards, the stack temperature decreases more gradually, primarily due to the condensation of water, which leads to the stabilization of the exergy flow.

The exergy flow through the stack is reduced more rapidly compared to the HPC outlet. The rise in exergy flow at the LPT outlet exceeds that at the combustor inlet, contributing to a reduction in exergy efficiency and an increase in exergy destruction within the black box. Once the stack temperature drops to 50 °C, the exergy loss via the stack stabilizes, leading to an improvement in exergy efficiency and a decrease in exergy destruction. This is shown by the double arrows in Fig. 8. The exergy gain in the heater (blue arrows) continues to increase after the flue gas condensation. However the exergy loss in cooler is increasing more gradually due to the stabilization of the stack exergy. Also the exergy loss in the intercooler diminishes at 28% of water-to-air ratio. As a result, at water amounts higher than 8%, the exergy efficiency increases but with a decreasing rate.

While the exergy efficiency initially decreases and then increases, the corresponding electrical efficiency of mGT behaves differently. It increases with the rise in injected water mass flow rate, as depicted

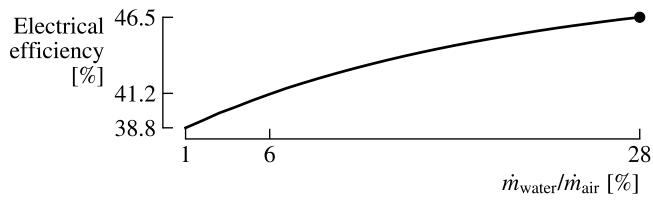


Fig. 9. 8.3% absolute efficiency increase is observed at the water injection limit ($SM_{LPC} = 10\%$).

in Fig. 9. The absolute efficiency gain is dependent on the amount of water injected. The rate of increase in efficiency as a function of the water fraction decreases and at 10% surge margin efficiency reaches 46.5% which is the maximum value (black dot in Fig. 9). The rate of increase reduces as water mass flow rate rises. This decrease in the efficiency rate of change is due to the shift of the operating point of the mGT. As the mGT operates at off-design both compressors present lower isentropic efficiencies towards the surge line. Also the isentropic efficiencies of the turbines are reducing from 84% for both to 79.9% for the HPT and 80.3% for the LPT as the Eq. (2) is applied.

At the maximum electrical efficiency the absolute efficiency increase is 8.3% from the dry case ($\eta_{el,dry} = 38.23\%$). Thus in the next section we will study if there is a possibility to reach this maximum efficiency limit using advanced humidified cycle configurations illustrating composite curves of their heat recovery system. From the electric and exergy efficiency results, it can be concluded that condensing the exhaust gases is essential to achieve such a high electrical efficiency. As a result the design of two-phase heat exchangers which recover the latent heat of flue gases should be considered.

4. Advanced humidified cycles

Various heat exchanger networks are modeled to evaluate their capability to reach the limit identified through the black box layout depicted in Fig. 4. 9 possible configurations are studied using advanced humidified cycle concepts and grouped in three main categories according to the literature review in the “Introduction” of this paper:

- Injection with complete water evaporation (Fig. 1(a)): It includes the conventional water injection at the outlet of the compression stage in a recuperated cycle (Fig. 10(a,b,c)). Configuration Fig. 10(a) applies direct water injection, Fig. 10(b) uses preheated liquid water from the economizer and Fig. 10(c) preheats the liquid water from the intercooler. Also more advanced concepts are studied. The REgenerative EVAPoration (REVA[®]) [26] cycle without aftercooling (see Fig. 10(d)) and the classic REVA[®] incorporating both intercooling and aftercooling (see Fig. 10(e)). In these cycles, a portion of the air/liquid water mixture after injection is employed for intercooling and/or aftercooling the compressor.
- Steam injection (Fig. 1(b)): The Steam Injected Gas Turbine (STIG) with auto-raised steam is selected to be injected in the recuperator inlet (Fig. 10(f)) and combustor inlet (Fig. 10(g)).
- Water injection through a humidification tower (Fig. 1(c)): This type includes the intercooled micro Humid Air Turbine (mHAT) cycle, where a saturation tower is incorporated for humidification between the HPC outlet and the recuperator inlet, see Fig. 10(h) and the Humid Air Turbine (HAT) [18] utilizing intercooling, aftercooling and the economizer to preheat the recirculated water before the injection into the saturation tower Fig. 10(i). This cycle is named HAT as it involves all the design aspects of this specific configuration, as patented by Rao [74]. Two-stage compression is combined with intercooler (IC), aftercooler (AC), recuperator and economizer (ECO) [74].

The selection is made considering specific operational criteria. Firstly, water is injected into the cycle to recover waste heat so the concept of liquid water injection into the combustion chamber to reduce NO_x emissions is not applied in this study. Also the water injection is located behind the compressor units, to avoid compressor damage. Thus wet compression with water droplets enter the compressors is not considered. Cycles that address the mass imbalance like the Cascaded Humidified Advanced Turbine (CHAT) [24] are not studied either. Finally, partial humidification is excluded since the primary objective is to maximize waste heat recovery.

Also according to De Paepe et al. the effectiveness of inlet air cooling using water atomization depends on the relative humidity of the inlet air as with a typical 60% relative humidity, the efficiency gains are limited [17]. When applied to the mHAT cycle, the effect of inlet air humidification on compressed air humidity at the compressor outlet is minimal due to the smaller water fraction added before the compressor compared to the saturation tower [17]. In summary, although inlet air cooling through fogging or WAC can improve the performance across all cycles, its efficiency is significantly influenced by the conditions of the inlet air. Moreover, inlet air cooling does not facilitate increased waste heat recovery [17]. Consequently, these methods are excluded from this study.

4.1. Modeling framework

The modeling of advanced humidified mGT cycles uses in-house model that was simulating the dry mGT cycle and is modified to accommodate humidification [49]. For the compressors, turbines and combustion chamber the same assumptions and boundary conditions are considered as in the black box analysis (Table 2). The heat exchangers were modeled using generic counter-flow heat exchanger model [17]. The pressure loss across the cold side of each component of the heat exchanger network was set to 1% of the total pressure, while a pressure drop of 3% was imposed on the hot side [64]. Furthermore, the feasibility of these values was verified through consultations with equipment manufacturers. The pressure loss is considered a design criterion as it directly impacts energy consumption and system efficiency, and is kept constant to allow for a consistent comparison across all simulation outcomes. Consequently, each finalized cycle design will require the creation of tailored heat exchangers to fulfill the specified heat transfer and pressure drop conditions.

The only change in boundary conditions of Table 2 involves the heat exchanger network. More specifically, the minimum pinch temperatures for the heat exchangers are:

- 50 °C (hot pinch) and 10 °C (cold pinch) for gas/gas at recuperator
- 10 °C for liquid/gas or gas-liquid/gas at economizer, intercooler, aftercooler and HRSG

Fig. 10 shows the components that adopt these minimum pinch temperatures with a star. If the intercooler component has black color, it means that it is not considered part of the humidification heat exchanger network and a 90% effectiveness is applied to it. Water enters the network at 15 °C and at the same pressure as the gas in the location of injection. Liquid water or steam injection uses an adiabatic mixer, introducing a 0.5% pressure loss that is presented in previous subsection. For cycles with humidified working fluids, a saturation tower simulated with the model that was described in Section 2.

For the simulations, 3 parameters are varied to converge into a solution for the cycle:

- Fuel flow rate regulates the turbine outlet temperature (TOT)
- Rotational speeds regulate the electrical power (P_{el})
- Water injection mass flow rater ($\dot{m}_{\text{feedwater}}$) regulates the minimum pinch

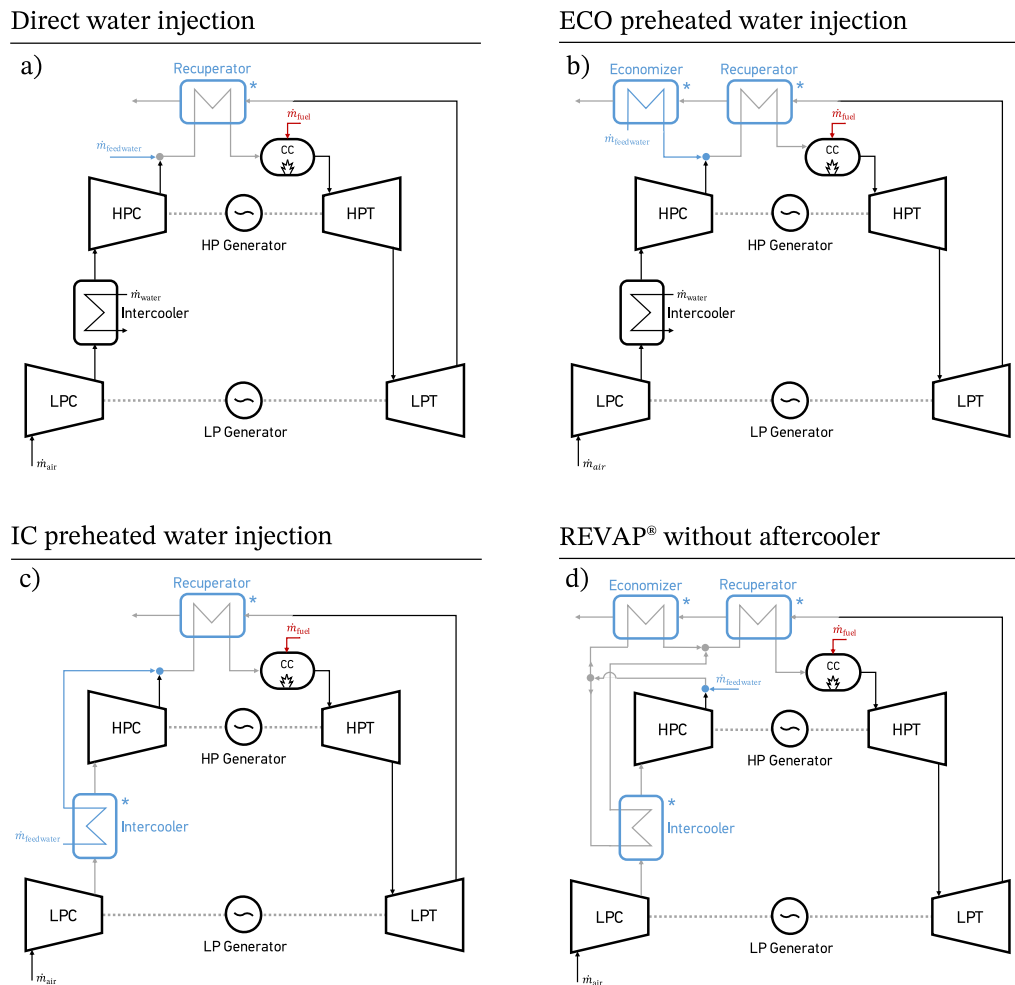


Fig. 10. Advanced humidified cycle configurations that are considered in this study. Liquid water, steam and water injection via a saturation tower are included. The components that are used in the heat exchanger network are indicated with a star.

To enhance the electrical efficiency of the mGT, the TOT is usually kept constant at 645 °C in most studied mGT cycles by adjusting the fuel flow rate [75]. Thus for the purposes of this study a TOT control with a constant temperature of 645 °C is applied. If, instead of maintaining TOT constant, TIT was kept fixed, as water is introduced, the TOT starts to increase which puts on risk the materials of heat exchanger. Therefore, a special consideration is required for the recuperator material selection [65]. To avoid this manufacturing constraint and apply realistic simulations, the TOT is kept constant. However that control choice decreases the TIT of the cycle with an increasing water injection rate and have a slight negative impact in the performance compared to a constant TIT [17]. This decrease of TIT is the result of the lower required energy by the fuel for the same electrical power output.

Simulations were performed using a constant electrical power output at 400 kW_e. The low-pressure and high-pressure rotational speeds are assumed to be equal as in the black box analysis which is a design choice at 400 kW_e [51]. When water or steam is injected downstream of the compressor, the mass imbalance between the compressor and turbine results in more power being available on the shaft, leading to an increase in power output. Consequently, the rotational speeds decrease, as the same power output can be achieved with a lower pressure ratio. Since the turbine is choked, the mGT's operating point shifts closer to the surge line, as depicted in Fig. 6. Therefore, a 10% surge margin is set as a minimum limit during the variation of rotational speeds.

The amount of water introduced into the cycle dictates the minimum pinches of the cycle. The model adjusts the feedwater flow rate to its maximum level, aligning with the point at which one component of the heat exchanger network attains its minimum pinch temperature (10 °C), while ensuring compliance with the other specified boundary conditions. For the mHAT, HAT, REVAP[®] without aftercooler and REVAP[®] cycle concepts, an additional control loop adjusts the water split fractions. For the mHAT and HAT, the split fractions are set to maximize the electrical efficiency. For the REVAP[®] cycles the air–water mixture is split between the economizer and the intercooler and/or aftercooler (Fig. 10(d,e)) to ensure equal temperatures in the cold-stream outlet of these components to minimize the exergy destruction.

The advanced humidified mGT cycles were evaluated against a dry cycle with intercooler water inlet temperature at 50 °C, intercooler effectiveness at 90% and a hot pinch of recuperator at 50 °C. This temperature is chosen assuming that the mGT is producing combined heat and power and thus is connected with the district heating system. This cycle presents 37.8% electrical efficiency, 34 780 rpm rotational speeds and air mass flow rate of 2.2 kg/s. The simulated efficiency is lower than the one presented by the authors of this paper [49] because of the increase in intercooler's return temperature (50 °C instead of 15 °C) and the TOT which is kept at 645 °C instead of 648.5 °C. In a next step the advanced humidified are also compared with the mGT that

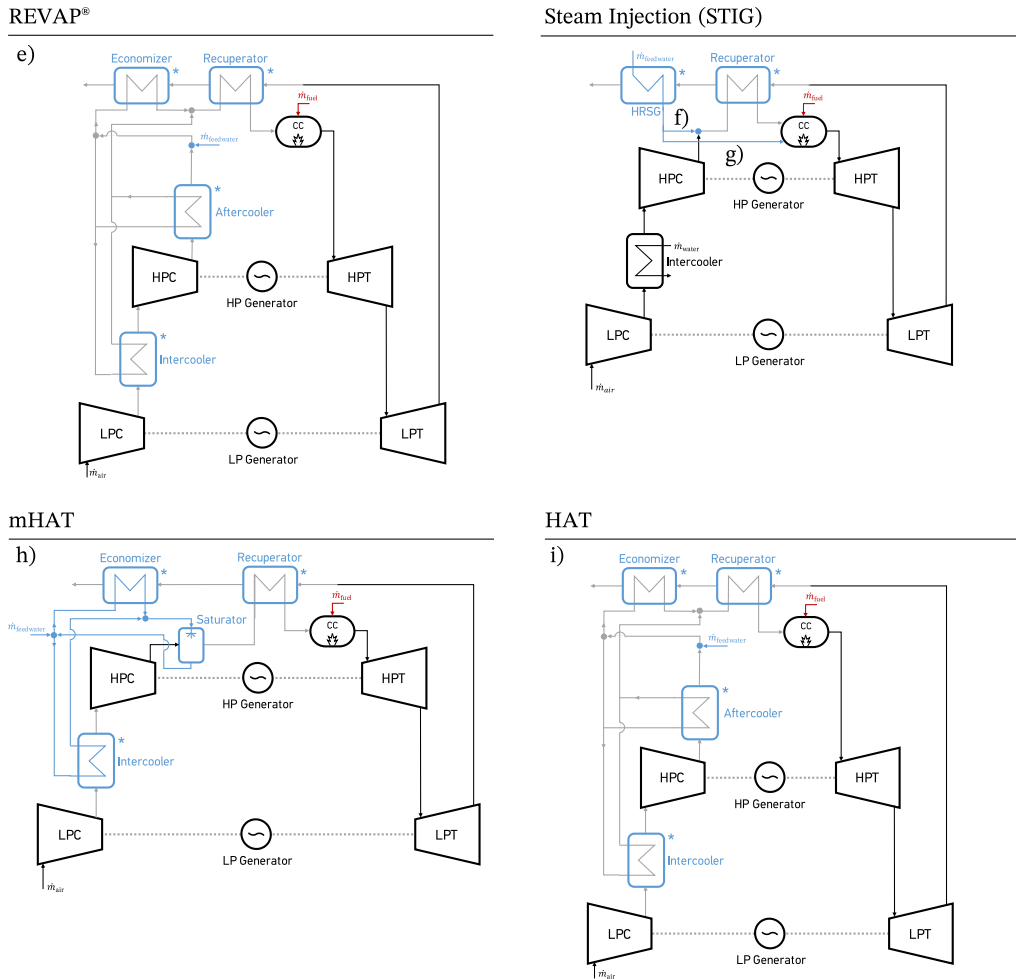


Fig. 10. (continued).

has an intercooler water inlet temperature at 15°C to compare basic intercooling versus humidification.

In addition to electrical performance, waste heat recovery is evaluated based on the amount of injected water and the flue gas temperature. Previous process-based simulations indicated maximizing the injected water improves recovery system efficiency, minimizing stack temperature. The total exergy flow of the exhaust gas serves as an alternative parameter for determining waste heat recovery [17]. For the mGT, a direct relationship exists between flue gas temperature and exergy flow. Higher water injection rates lower stack temperatures and total mass flow rates (due to turbine choking), resulting in lower exergy flow rates.

4.2. Advanced humidified cycles results

Examination of the simulation results in Fig. 11, 12 for the proposed cycles (Fig. 10) shows that the layout achieving the lowest stack temperature, maximizing waste heat recovery, provides the highest cycle efficiency (Fig. 11). It is shown that the REVAP® cycle concept presents the highest efficiency increase of 4.1% points (shown with light blue color in Fig. 11) as it condenses the flue gasses (see dew point temperature at Fig. 12). The HAT cycle follows closely with comparable efficiency increase but with higher injected water amount and higher stack temperature (Fig. 12). The mHAT is in the third place with an efficiency increase of 3.1% and the REVAP® without aftercooler follows with 3.0%. The preheated liquid water injection (WI) from economizer presents 2.6% efficiency increase and performs better than the direct WI (2.5%) and preheated WI from IC (2% points). Although

the REVAP® has a more complex layout, its efficiency gain is not significantly higher than that of the simpler preheated water injection, with a difference of just 1.5 percentage points. The use of an aftercooler in HAT configuration achieves an 0.9% higher efficiency the concept without and aftercooler (mHAT). The REVAP® also shows 1.1% increase with the use of aftercooler. This certifies that the utilization of aftercooling adding an extra 1% in the efficiency. Whereas none of the concepts reach the water injection limit as outlined in the black box analysis from the previous section.

The STIG concept with steam injection in the combustion chamber yields the smallest increase in cycle efficiency at just 0.1% points. The STIG with injection in the recuperator inlet performs better (1.4% points increase) due to the increased heat recovery in the recuperator. Although, both of STIG concepts show less promising results than the other cycles. This lower performance in STIG is due to high exergy destruction in the HRSG [17]. This demonstrates that advanced direct water injection (REVAP® cycles) for 2-spool mGT humidification ((Fig. 10(c,d)) is in terms of waste heat recovery and electrical efficiency similar compared to humidification using a saturation tower ((Fig. 10(h,i)).

While the efficiency improvements are analyzed, it is also important to consider the impact of rotational speed variation on the air mass flow rate (\dot{m}_{air}). As seen in Fig. 11, changes in RPM and especially the significant reductions observed for high-performing cycles like REVAP and HAT can directly influence the compressor's operating point and, consequently, the air mass flow. The reduction of air mass flow rate is 16.4% and 17.3% for the REVAP and HAT, respectively. Furthermore the decrease of air mass flow rate is not only affected by the reduction

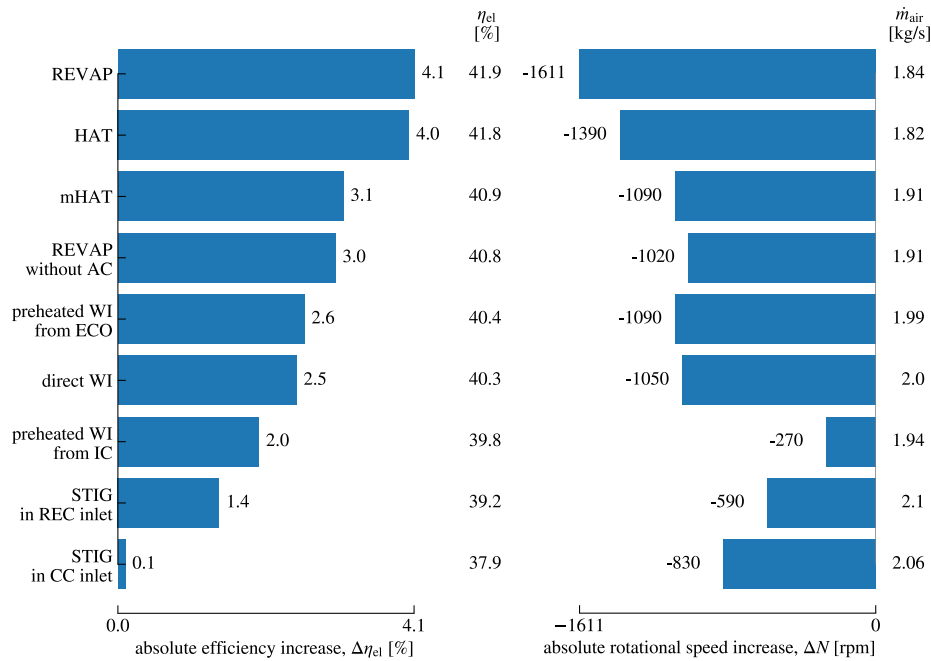


Fig. 11. The REVAP[®] concept shows the highest efficiency increase followed closely by the HAT as both taking advantage of the pre-injection aftercooling. Liquid water injection has 1.5% points lower efficiency than REVAP[®] regardless the increased complexity of the latter concept. REVAP[®] has the lowest rotational speed which is linked with the most effective waste heat recovery.

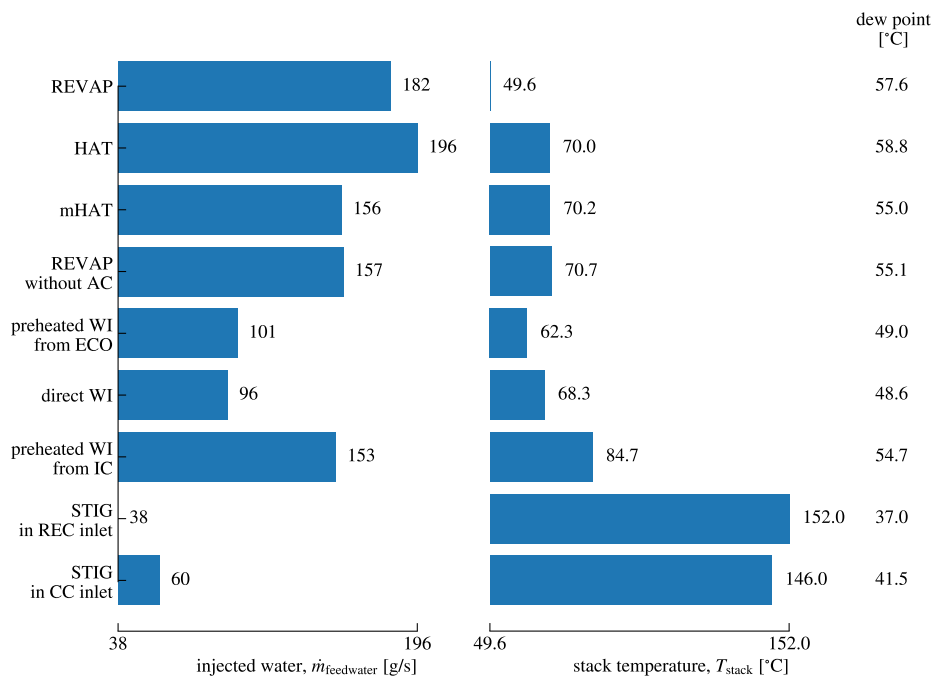


Fig. 12. HAT shows the highest injected water but not the lowest stack. The injected water increases the turbine work but the heat recovery is slightly lower than the REVAP[®] resulting in similar performances. REVAP[®] is the only cycle that condenses the flues gases.

of rotational speed of the cycle but it is also linked with the amount of water that is injected. Therefore the injected water of Fig. 12 is inversely proportional to the air mass flow rate of the cycle as the LP and HP turbines are choked.

The REVAP[®] cycle concept achieves the lowest stack temperature at 49.6 °C, resulting in the highest electrical efficiency increase of 4.1% points among all the cycles analyzed. Nevertheless, this peak in efficiency and waste heat recovery still does not meet the exergetic limit identified in the black box analysis. This analysis indicated that

400 g/s of water injection could yield an electrical efficiency of 46.5% at a constant power output of 400 kW_e (Fig. 9). However, the limitation is imposed by the LPC, which reaches a 10% surge margin (Fig. 6), rather than by any violation of the second law of thermodynamics. The exergetic efficiency of the heat recovery network remains below the 93% threshold, with exergy destruction exceeding the minimal 5%. This indicates that, from a thermodynamic perspective, it might be possible to inject more water, but doing so would necessitate redesigning the compressor. More specifically, the REVAP[®] cycle shows an exergy

efficiency in the heat exchanger network of 87.5% with an exergy destruction of 9.8%. From this, two key points can be inferred. Firstly, it might be possible to design a heat exchanger network that optimizes waste heat recovery. The primary challenge is in capturing the condensation heat of water, which is necessary to attain an exergetic heat recovery efficiency of 93%. In the mGT equipped with the REVAP[®] concept, the stack temperature drops below the dew point (Fig. 12), indicating that a portion of the condensation heat from the water in the stack is recovered. However, achieving the black box limit requires capturing an even larger portion of this condensation heat. The difficulty lies in recovering substantial amounts of heat available at low temperatures (below 57.6 °C), which presents significant challenges. This is feasible only if the cold stream has a mass flow rate several magnitudes higher than the flue gas mass flow rate (which is not possible in this scenario) or if combined with a phase-change process [17]. Although the latter is achieved by the REVAP[®] cycle, more condensation is required to reach this exergetic efficiency limit which is impossible with this designed configuration. Secondly, the limits set by the black box analysis (93% exergetic efficiency and 5% exergy destruction) may be overly ambitious even for 2-spool mGTs. Due to the lower maximum allowable TOT of 645 °C, mGTs operate with a much higher air-to-fuel ratio than large-scale GTs. This higher air-to-fuel ratio results in a greater energy flow within the heat exchanger network of humidified cycles compared to the energy input from the fuel in the combustion chamber (even in the dry cycle, both energy flows are of a similar magnitude). In contrast, large GTs operate at higher TITs (over 1500 °C [76]) with a lower air-to-fuel ratio. Consequently, the larger air-to-fuel ratio in mGTs stores more energy at lower temperatures (low exergy), leading to potentially higher exergy destruction during heat recovery. Therefore, it is likely that the limits need to be adjusted for the mGT scale. This observation aligns with previous studies on simple recuperated mGTs by the research group [33], where the only cycle capable of achieving such exergy efficiency was the M-power, though it required an unrealistic wet-bulb effectiveness of 98%, which is practically not feasible [77].

The impact of feedwater preheating on the overall cycle performance for liquid water injection concepts is relatively minor (Fig. 11). Preheating the feedwater using an economizer yields only a 0.1% increase in efficiency compared to direct water injection. This modest effect is attributed to the low mass flow rates of feedwater, which restrict the amount of waste heat that can be recovered. However, while there is a slight positive impact, the inclusion of an additional preheater in the final cycle design should be carefully considered. Given its minimal influence on performance, the added cost of such a component may not be justified. Moreover the preheated water injection from IC shows worse performance than the direct water injection by 0.5% points (Fig. 11). This is associated with the fact that the IC component influences the required work of the compressor depending on how well it cools down the HPC inlet. As the air is cooled through the IC, the required HPC work is reduced, consequently the electrical efficiency is increased. In this concept the temperature of HPC inlet drops only to 109 °C (see Fig. A.1 - Preheat water injection from IC) due to the small mass flow rate of feedwater. Therefore, the efficiency of the preheated water injection from IC under-performs compared to the other liquid water injection configurations.

Composite curves identify the limitations of the components based on the pinch. They illustrate the heat exchange between hot and cold streams across various temperatures. They also demonstrate the amount of heat transferred between the streams and the associated temperature changes during the heat transfer process. Fig. 13 shows the composite curves of all the heat exchanger units side by side and also combined for REVAP[®], HAT and STIG concepts. The composite curves of the others concepts are presented in Appendix (Fig. A.1). Combining the composite curves of different heat exchanger networks provides insight into different cycle performances. Additionally, presenting each composite

curve side by side for each heat exchanger component allows for a detailed examination of the specific behavior and interactions within each unit. This dual presentation method provides valuable insights into the effectiveness of the heat exchanger networks in different configurations. The width along the *x*-axis of Fig. 13 represents the total energy transferred by the hot stream and absorbed by the cold stream. For optimal performance, the cold and hot curves should be as close as possible, ideally separated by the pinch temperature of 10 °C, across the entire temperature range.

As shown in Fig. 13, the REVAP[®] cycle achieves the highest heat recovery of 1711 kW, evident from the very low starting temperature of the cold curve and the minimal distance between the hot and cold curves. These composite curves also explain why STIG (Fig. 13 bottom curves) consistently performs worse compared to water injection, both with and without a saturation tower. As feedwater reaches its boiling point, its temperature remains constant during steam generation in the HRSG, determined by the water pressure, until complete evaporation occurs. During this boiling phase, the cold stream absorbs heat from the hot stream to vaporize the liquid water, causing the hot stream to cool while the cold stream's temperature remains unchanged (isothermal process). Thus the amount of water is dictated by the isothermal process which gives high amounts of heat as vaporizes the feedwater. If the water mass flow rate increase further, the composite curves will cross. As a result the STIG configurations show high temperature difference in the combined composite curves. Conversely, cycles utilizing water injection (Fig. A.1) do not face this restriction. The saturation tower in these cycles can achieve smaller overall temperature differences in the composite curves (Fig. 13 - HAT), leading to greater heat exchange and improved cycle performance, as evaporation occurs across a range of temperatures.

Simulation results reveal that direct water injection using the REVAP[®] method, which allows for complete evaporation, performs slightly better than cycle humidification via a saturation tower (HAT concept). Direct injection cools the hot compressed air through rapid evaporation, creating a two-phase flow mixture that aids in heat recovery and improves cycle performance. However, two-phase flow complicates heat exchanger design, making heat transfer behavior challenging to predict. The dynamics of two-phase flow are also challenging to predict and model, as its presence could lead to imbalances in heat exchangers [78]. If varying liquid fractions enter different channels, each may experience a different temperature, causing an imbalance. Depending on the gas/liquid fraction, multiple flow regimes can emerge, with differing flow characteristics and heat transfer behavior. When water injection is limited to prevent two-phase flow, the amount is capped at 49 and 43 g/s for preheated and direct injection, respectively, yielding efficiency gains of 1.3 and 1.1%.

Moreover considering the case that the mGT does not add further heat exchangers than those it already presents for its function in CHP concepts, the heat exchangers are limited to three (intercooler, recuperator, economizer). In this scenario, mHAT cycle is far superior than all the other configurations providing the highest efficiency, lowest stack temperature (70.2 °C) and highest amounts of feedwater. As a result the optimal recoverable heat is achieved with the mHAT.

In terms of practical implementation, recent economic analysis confirms the potential viability of mHAT cycles under favorable conditions. Montero Carrero et al. [79] conducted a comparative study of mGT, ICE, and mHAT technologies in small-scale cogeneration across several European countries. Their results indicate that, although current policies are generally insufficient for widespread feasibility, mHAT cycles deliver the highest potential revenues when profitability is achieved. Notably, in regions with supportive subsidies — such as Brussels — the mHAT configuration approaches economic viability. This confirms that advanced humidified cycles like mHAT are not only thermodynamically promising, but may also become economically viable with adequate policy support and market conditions.

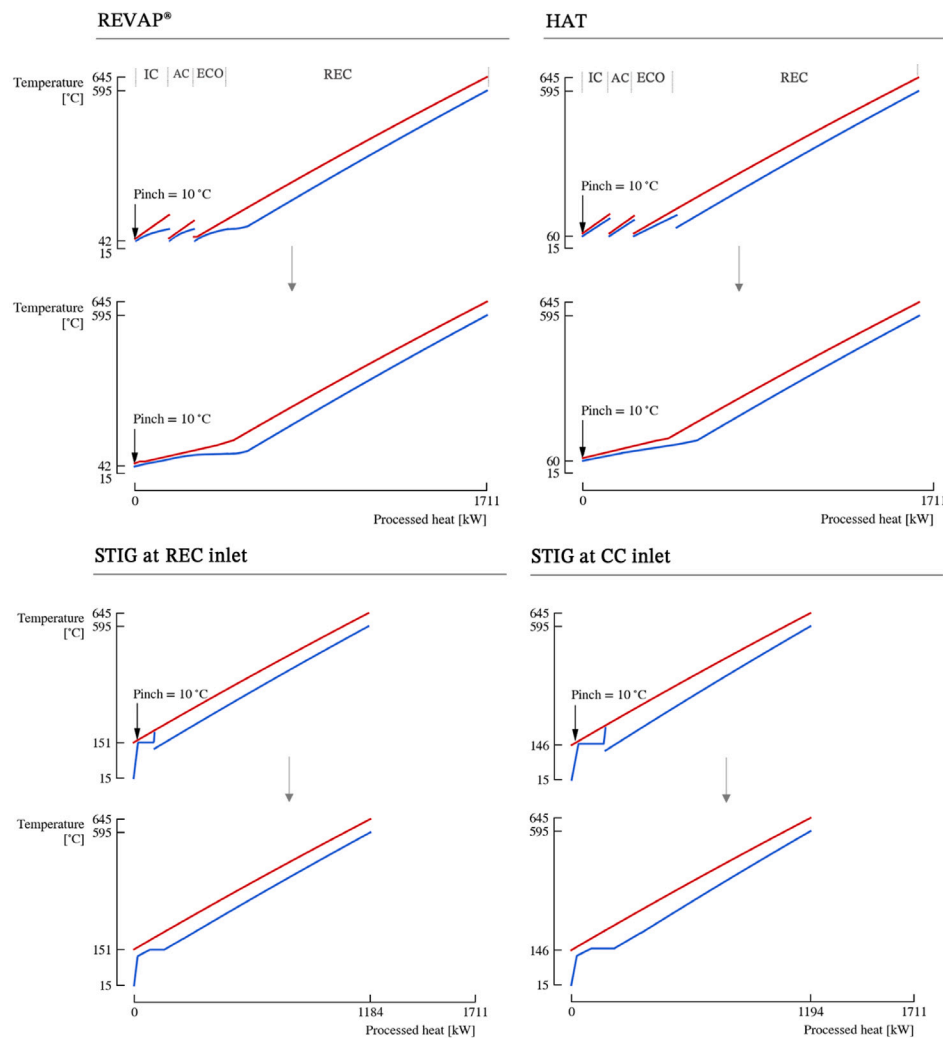


Fig. 13. Composite curves for REVAP[®], HAT and STIG concepts. The curves of each component and the combined curves are shown to identify the pinch and the processed heat. REVAP[®] shows the highest recovered heat as it presents the highest performance.

It is important to note, however, that the values presented here do not consider the use of actual heat exchangers (without fixed hot pinch but with fixed surface). If only the existing heat exchangers were used, the performance would be lower. Thus, REVAP[®] scenarios outperform cycle concepts utilizing a saturation tower for humidification only when two-phase flow is permitted. If two-phase flow is restricted, cycle concepts with saturation towers demonstrate the greatest potential.

5. Conclusions

In this paper we presented the results of simulations focusing on advanced humidification in a 2-spool mGT. A two-step method was utilized to identify the optimal thermodynamic conditions for water injection. The key findings are categorized below:

1. Black box analysis: At first, the heat exchanger network of the mGT was replaced with a black box system. The black box simulations indicated that a 8.3% absolute increase in efficiency could be obtained by injecting 28% wt of water-to-air ratio (400 g/s) into the HPC outlet without violating the second law of thermodynamics.

2. Advanced humidified cycles analysis: In the next step, multiple advanced humidified mGT concepts are simulated to assess their potential for waste heat recovery. This study demonstrates that advanced humidification strategies in a 2-spool mGT, specifically using

the REVAP[®] cycle, can significantly enhance efficiency through optimized water injection and waste heat recovery. The REVAP[®] cycle is found to achieve the highest efficiency increase by effectively condensing flue gases and lowering stack temperatures, though it involves a more complex setup than simpler configurations. Moreover, it still falls short of the exergetic limit found in black box analysis due to design limitations set by the mGT cycle.

3. Design and manufacturing considerations: If two-phase flow is avoided and the heat exchanger components are limited to be higher than 3 units, the mHAT cycle delivers the best performance, showing the importance of careful cycle design in optimizing mGT systems. While two-phase flow enables higher heat recovery, it complicates heat exchanger design. If two-phase flow is restricted, saturation tower concepts hold the greatest potential. Overall, these findings underscore that cycle layout and design considerations play crucial roles in maximizing mGT performance.

4. Future perspectives: A sensitivity analysis examining the influence of key operating parameters — such as water injection rate, temperature, and pressure — on cycle performance would provide valuable insight into the robustness and practical applicability of the proposed configurations. Future work should also prioritize testing other advanced configurations, such as AHAT and CHAT cycles, and assess operational risks in transient conditions for mHAT cycles. Additionally, the potential of alternative fuels in humidified cycles warrants

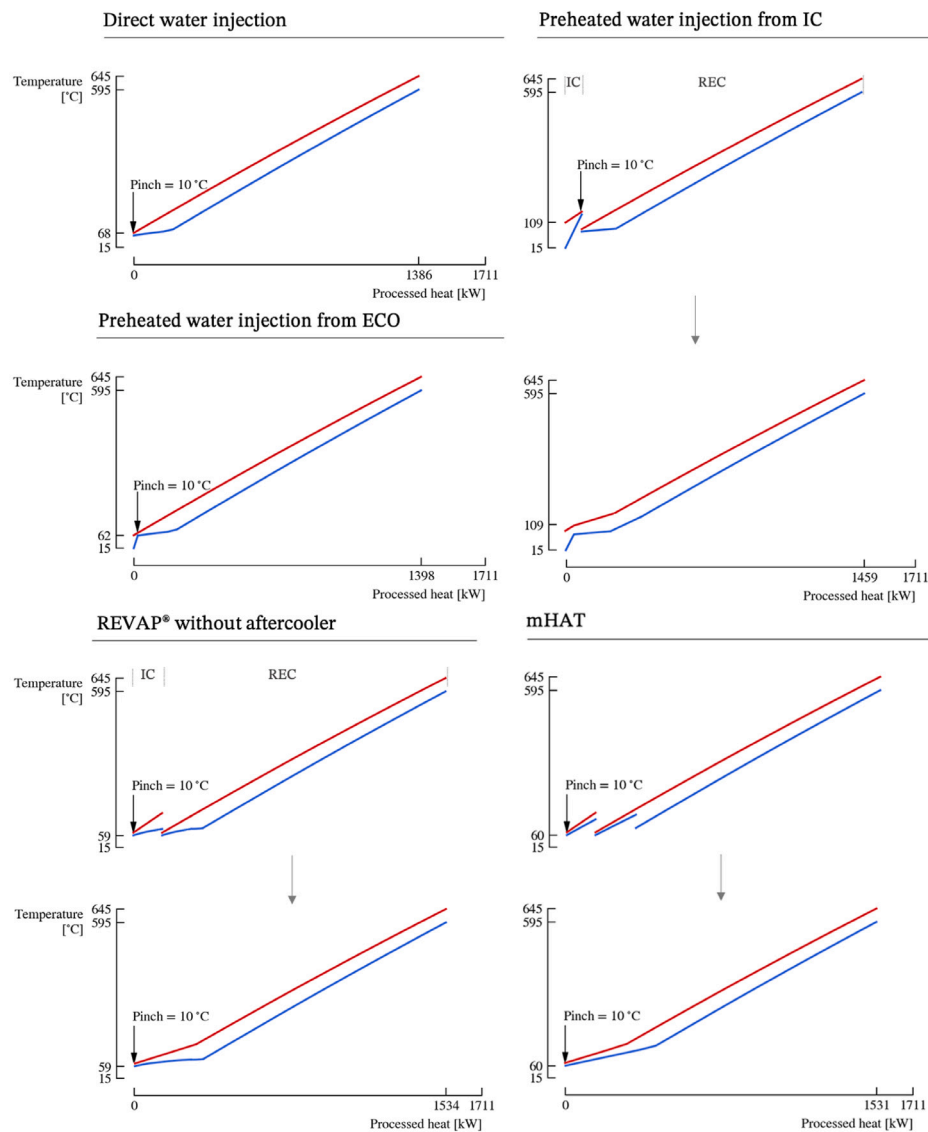


Fig. A.1. Composite curves for liquid water injection, REVAP[®] without AC and mHAT concept.

exploration to address performance limitations, especially in the compressor and combustion chamber. Manufacturing and experimental testing of a saturation tower on a 2-spool mGT is underway and can further validate the simulated performance improvements presented here.

CRediT authorship contribution statement

Aggelos Gaitanis: Writing – original draft, Visualization, Validation, Software, Methodology, Investigation, Formal analysis. **Francesco Contino:** Writing – review & editing, Supervision, Funding acquisition. **Ward De Paepe:** Writing – review & editing, Supervision, Project administration, Data curation, Conceptualization.

Declaration of competing interest

The authors declare that they have no known competing financial interests or personal relationships that could have appeared to influence the work reported in this paper.

Acknowledgments



Co-funded by the
European Union

The authors would like to acknowledge the financial support received from the European Union's Horizon 2020 research and innovation programme under grant agreement No. 861079 (NextMGT – Next Generation of Micro Gas Turbines for High Efficiency, Low Emissions, and Fuel Flexibility, Belgium) and European Union's grant agreement No. 101083536 (Fit4Micro - Clean and efficient micro CHCP by micro turbine based hybrid systems, Belgium). Views and opinions expressed are however those of the authors only and do not necessarily reflect those of the European Union or CINEA. Neither the European Union nor the granting authority can be held responsible for them.

Appendix

See Fig. A.1.

Data availability

Data will be made available on request.

References

- [1] Heppenstall T. Advanced gas turbine cycles for power generation: A critical review. *Appl Therm Eng* 1998;18:837–46.
- [2] Samitha Weerakoon A, Assadi M. Trends and advances in micro gas turbine technology for sustainable energy solutions: A detailed review. *Energy Convers Manag*; X 2023;20:100483. <http://dx.doi.org/10.1016/j.ecmx.2023.100483>, URL <https://linkinghub.elsevier.com/retrieve/pii/S2590174523001393>.
- [3] De Paepe W, Montero Carrero M, Bram S, Parente A, Contino F. Toward higher micro gas turbine efficiency and flexibility—Humidified micro gas turbines: A review. *ASME J Eng Gas Turbines Power* 2018;140(8):081702. <http://dx.doi.org/10.1115/1.4038365>, Publisher: American Society of Mechanical Engineers (ASME).
- [4] Jonsson M, Yan J. Humidified gas turbines: A review of proposed and implemented cycles. *Energy* 2005;30:1013–78.
- [5] Hamdan Al Assaf A, Amhamed A, Fawwaz Alrebei O. State of the art in humidified gas turbine configurations. *Energies* 2022;15(24). <http://dx.doi.org/10.3390/en15249527>, URL <https://www.mdpi.com/1996-1073/15/24/9527>.
- [6] Alhazmy M, Najjar Y. Augmentation of gas turbine performance using air coolers. *Appl Therm Eng* 2004;24:415–29.
- [7] Saghafifar M, Gadalla M. Innovative inlet air cooling technology for gas turbine power plants using integrated solid desiccant and Maisotsenko cooler. *Energy* 2015;87:663–77. <http://dx.doi.org/10.1016/j.energy.2015.05.035>, URL <https://www.sciencedirect.com/science/article/pii/S0360544215006167>.
- [8] Bhargava R, Bianchi M, Campanari S, Pascale A, Montenegro G, Peretto A. High efficiency gas turbine based power cycles—A study of the most promising solutions: Part 1—A review of the technology. In: *Proceedings of the ASME turbo expo 2008: power for land, sea, and air*, vol. 43178, Berlin, Germany; 2008, p. 305–14.
- [9] Roumeliotis I, Mathioudakis K. Evaluation of water injection effect on compressor and engine performance and operability. *Appl Energy* 2010;87:1207–16.
- [10] Wang F, Chiou J-S. Performance improvement for a simple cycle gas turbine GENSET—a retrofitting example. *Appl Therm Eng* 2002;22:1105–15.
- [11] Ingistov S. Interstage injection into axial compressor, gas turbine model 7EA: Part 2. In: *Proceedings of the ASME turbo expo 2002: power for land, sea, and air*, vol. 36096, Amsterdam, The Netherlands; 2002.
- [12] Zheng Q, Sun Y, Li S, Wang Y. Thermodynamic analyses of wet compression process in the compressor of gas turbine. *J Turbomach* 2003;125:489–96.
- [13] Chaker M, Meher-Homji CB, Mee III T. Inlet fogging of gas turbine engines—Part I: Fog droplet thermodynamics, heat transfer, and practical considerations. *J Eng Gas Turbines Power* 2004;126(3):545–58. <http://dx.doi.org/10.1115/1.1712981>.
- [14] Kang S, Kim J, Kim T. Influence of steam injection and hot gas bypass on the performance and operation of a combined heat and power system using a recuperative cycle gas turbine. *J Mech Sci Technol* 2013;27:2547–55.
- [15] Nishida K, Takagi T, Kinoshita S. Regenerative steam-injection gas-turbine systems. *Appl Energy* 2005;81:231–46.
- [16] Traverso A, Massardo A. Thermo-economic analysis of mixed gas-steam cycles. *Appl Therm Eng* 2002;22:1–21.
- [17] De Paepe W, Montero Carrero M, Bram S, Contino F, Parente A. Waste heat recovery optimization in micro gas turbine applications using advanced humidified gas turbine cycle concepts. *Appl Energy* 2017;207:218–29. <http://dx.doi.org/10.1016/j.apenergy.2017.06.001>, URL <https://linkinghub.elsevier.com/retrieve/pii/S0306261917307511>.
- [18] Gallo W. A comparison between the HAT cycle and other gas-turbine based cycles: Efficiency, specific power and water consumption. *Energy Convers Manage* 1997;38:1595–604.
- [19] De Ruyck J, Bram S, Allard G. Humid air cycle development based on exergy analysis and composite curve theory. 1995, ASME Pap Nr. 95- CTP-39, 1995.
- [20] Kim T, Song C, Ro S, Kauh S. Influence of ambient condition on thermodynamic performance of the humid air turbine cycle. *Energy* 2000;25:313–24.
- [21] Lazzaretto A, Segato F. Thermodynamic optimization of the HAT cycle plant structure - part I: Optimization of the basic plant configuration. *J Eng Gas Turbines Power* 2001;123:1–7.
- [22] Lazzaretto A, Segato F. A thermodynamic approach to the definition of the HAT cycle plant structure. *Energy Convers Manage* 2002;43:1377–91.
- [23] Hatamiya S. Advanced humid air turbine system. In: *The 7th national symposium on power and energy systems of JSME*. Tokyo, Japan; 2000, p. 13–6.
- [24] Nakhamkin M, Swensen E, Wilson J, Gaul G, Polsky M. The cascaded humidified advanced turbine (CHAT). *J Eng Gas Turbines Power* 1996;118:565–71.
- [25] Van Liere J, Laagland G. The TOPHAT® cycle. *VDI-Ber* 2000;161–75.
- [26] De Ruyck J, Bram S, Allard G. REVAP® cycle: A new evaporative cycle without saturation tower. *J Eng Gas Turbines Power* 1997;119:893–7.
- [27] News releases : February 14, 2013 : Hitachi global. 2013, URL <https://www.hitachi.com/New/cnews/130214.html>.
- [28] De Paepe W, Carrero MM, Bram S, Parente A, Contino F. Experimental characterization of a t100 micro gas turbine converted to full humid air operation. *Energy Procedia* 2014;61:2083–8.
- [29] Brandon R, Halliday B, Hoffman JS. Inlet air supercharging of a 70 kw microturbine. In: *Proceedings of ASME turbo expo 2006*. 2006, p. 353–8, Issue: GT2006-90555.
- [30] Dodo S, Nakano S, Inoue T, Ichinose M, Yagi M, Tsubouchi K, et al. Development of an advanced microturbine system using humid air turbine cycle. In: *ASME conference proceedings, ASME paper GT2004-54337*. 2004, p. 167–74.
- [31] Renzi M, Caresana F, Pelagalli L, Comodi G. Enhancing micro gas turbine performance through fogging technique: Experimental analysis. *Appl Energy* 2014;135:165–73. <http://dx.doi.org/10.1016/j.apenergy.2014.08.084>, URL <https://linkinghub.elsevier.com/retrieve/pii/S0306261914008952>.
- [32] De Paepe W, Delattin F, Bram S, De Ruyck J. Water injection in a micro gas turbine – assessment of the performance using a black box method. *Appl Energy* 2012;112:1291–302.
- [33] De Paepe W, Contino F, Delattin F, Bram S, De Ruyck J. Optimal waste heat recovery in micro gas turbine cycles through liquid water injection. *Appl Therm Eng* 2014;70(1):846–56.
- [34] Zhang S, Xiao Y. Steady state off-design thermodynamic performance analysis of a humid air turbine based on a micro turbine. In: *Proceedings of ASME turbo expo 2006*. 2006, p. 287–96, Issue: GT2006-90335.
- [35] Lee JJ, Jeon MS, Kim TS. The influence of water and steam injection on the performance of a recuperated cycle microturbine for combined heat and power application. *Appl Energy* 2010;87:1307–16.
- [36] Mochizuki K, Shibata S, Inoue U, Tsuchiya T, Sotouchi H, Okamoto M. New concept of a micro gas turbine based co-generation package for performance improvement in practical use. In: *ASME conference proceedings, ASME paper PWR2005-50364*. 2005, p. 1305–10.
- [37] Ferrari ML, Pascenti M, Traverso AN, Massardo AF. Hybrid system test rig: Chemical composition emulation with steam injection. *Appl Energy* 2012;97:809–15.
- [38] De Paepe W, Delattin F, Bram S, Contino F, De Ruyck J. A study on the performance of steam injection in a typical micro gas turbine. In: *Proceedings of the ASME turbo expo 2013*. 2013, Issue: GT2013-94569.
- [39] Parente J, Traverso A, Massardo AF. Micro humid air cycle: Part a - thermodynamic and technical aspects. In: *ASME conference proceedings, ASME paper GT2003-38326*. 2003, p. 221–9.
- [40] Xu Z, Lu Y, Wang B, Zhao L, Xiao Y. Experimental study on the off-design performances of a micro humid air turbine cycle: Thermodynamics, emissions and heat exchange. *Energy* 2021;219:119660. <http://dx.doi.org/10.1016/j.energy.2020.119660>, URL <https://www.sciencedirect.com/science/article/pii/S0360544220327675>.
- [41] Parente J, Traverso A, Massardo AF. Micro humid air cycle: Part b - thermo-economic analysis. In: *ASME conference proceedings, ASME paper GT2003-38328*. 2003, p. 231–9.
- [42] Montero Carrero M. Decoupling heat and electricity production from micro gas turbines: numerical, experimental and economic analysis of the micro humid air turbine cycle [Ph.D. thesis], Vrije Universiteit Brussel, Université Libre de Bruxelles; 2018.
- [43] Wan K, Zhang S, Wang J, Xiao Y. Performance of humid air turbine with exhaust gas expanded to below ambient pressure based on microturbine. *Energy Convers Manage* 2010;51(11):2127–33.
- [44] Pashchenko D, Mustafin R, Karpilov I. Thermochemical recuperation by steam methane reforming as an efficient alternative to steam injection in the gas turbines. *Energy* 2022;258:124913. <http://dx.doi.org/10.1016/j.energy.2022.124913>, URL <https://www.sciencedirect.com/science/article/pii/S0360544222018138>.
- [45] Pashchenko D. Thermochemical waste-heat recuperation by steam methane reforming with flue gas addition. *Int J Energy Res* 2019;43(6):2216–26. <http://dx.doi.org/10.1002/er.4436>, URL <https://onlinelibrary.wiley.com/doi/abs/10.1002/er.4436>, eprint: <https://onlinelibrary.wiley.com/doi/pdf/10.1002/er.4436>.
- [46] Pashchenko D, Mustafin R, Karpilov I. Efficiency of chemically recuperated gas turbine fired with methane: Effect of operating parameters. *Appl Therm Eng* 2022;212:118578. <http://dx.doi.org/10.1016/j.applthermaleng.2022.118578>, URL <https://www.sciencedirect.com/science/article/pii/S1359431122005270>.
- [47] De Ruyck J, Delattin F, Bram S. Co-utilization of biomass and natural gas in combined cycles through primary steam reforming of the natural gas. In: *Energy, ECOS 05. 18th international conference on efficiency, cost, optimization, simulation, and environmental impact of energy systems*, vol. 32, no. 4, 2007, p. 371–7. <http://dx.doi.org/10.1016/j.energy.2006.07.010>, URL <https://www.sciencedirect.com/science/article/pii/S0360544206001940>.
- [48] El-Masri MA. A modified, high-efficiency, recuperated gas turbine cycle. *J Eng Gas Turbines Power* 1988;110:233–42.
- [49] Gaitanis A, Tiwari RN, De Paepe W, Ferrari ML, Contino F, Breuhaus P. Operational strategies of two-spool micro gas turbine with alternative fuels: A performance assessment. *J Eng Gas Turbines Power* 2024;146(091011). <http://dx.doi.org/10.1115/1.4064798>.

- [50] Aurelia Turbines. Aurelia turbines official website. 2023, <https://aureliaturbines.com/>. [Accessed 20 December 2023].
- [51] Jaatinen-Värri A, Nerg J, Uusitalo A, Ghalamchi B, Uzhegov N, Smirnov A, et al. Design of a 400 kW gas turbine prototype. In: Volume 8: microturbines, turbochargers and small turbomachines; steam turbines. Seoul, South Korea: American Society of Mechanical Engineers; 2016, <http://dx.doi.org/10.1115/GT2016-56444>, URL <https://asmedigitalcollection.asme.org/GT/proceedings/GT2016/49866/Seoul,%20South%20Korea/241113,V008T23A007>.
- [52] Cengel YA, Boles MA. Thermodynamics: an engineering approach. McGraw Hill; 2006.
- [53] Parente J, Traverso A, Massardo A. Micro humid air cycle: Part a – thermodynamic and technical aspects. In: Proceedings of ASME turbo expo 2003. ASME; 2003, p. 221–9.
- [54] Sher AA, Ahmad N, Sattar M, Phelan P, Lin A. Computational analysis of multi-fuel micro-gas turbine annular combustion chamber. *J Therm Anal Calorim* 2024;149(8):3317–29. <http://dx.doi.org/10.1007/s10973-024-12924-z>.
- [55] Goodwin DG, Moffat HK, Schoegl I, Speth RL, Weber BW. Cantera: An object-oriented software toolkit for chemical kinetics, thermodynamics, and transport processes. 2023, <http://dx.doi.org/10.5281/zenodo.8137090>, URL <https://zenodo.org/records/8137090>.
- [56] Belokon AA, Khritov KM, Klyachko LA, Tschepin SA, Zakharov VM, Opdyke JG. Prediction of combustion efficiency and NOx levels for diffusion flame combustors in hat cycles. In: ASME conference proceedings. 2002, p. 791–7.
- [57] Bell IH, Wronski J, Quoilin S, Lemort V. Pure and pseudo-pure fluid thermophysical property evaluation and the open-source thermophysical property library CoolProp. *Ind Eng Chem Res* 2014;53(6):2498–508. <http://dx.doi.org/10.1021/ie4033999>, URL <http://pubs.acs.org/doi/abs/10.1021/ie4033999>. eprint: <http://pubs.acs.org/doi/pdf/10.1021/ie4033999>.
- [58] Virtanen P, Gommers R, Oliphant TE, Haberland M, Reddy T, Cournapeau D, et al. Scipy 1.0: Fundamental algorithms for scientific computing in python. *Nature Methods* 2020;17:261–72. <http://dx.doi.org/10.1038/s41592-019-0686-2>.
- [59] Fredenslund A. Vapor-Liquid Equilibria Using Unifac: a Group-Contribution Method. Amsterdam: Elsevier Science; 2014, URL <http://qut.eblib.com.au/patron/FullRecord.aspx?p=1179913>, OCLC, 1044727515.
- [60] Lemmon EW, Bell IH, Huber ML, McLinden MO. NIST standard reference database 23: Reference fluid thermodynamic and transport properties-REFPROP, version 10.0, national institute of standards and technology. 2018, <http://dx.doi.org/10.18434/T4/1502528>, URL <https://www.nist.gov/srd/refprop>.
- [61] Aspen plus | leading process simulation software | AspenTech. 2023, URL <https://www.aspentech.com/en/products/engineering/aspens-plus>.
- [62] Montero Carrero M, De Paepe W, Bram S, Contino F. Thermodynamic analysis of water injection in a micro gas turbine: Sankey and grassmann diagrams. *Energy Procedia* 2017;105:1414–9. <http://dx.doi.org/10.1016/j.egypro.2017.03.527>, URL <https://linkinghub.elsevier.com/retrieve/pii/S1876610217305726>.
- [63] Hashmi MB, Mansouri M, Assadi M. Dynamic performance and control strategies of micro gas turbines: State-of-the-art review, methods, and technologies. *Energy Convers Manag* X 2023;18:100376. <http://dx.doi.org/10.1016/j.ecmx.2023.100376>.
- [64] Malkamäki M, Jaatinen-Värri A, Honkatukia A, Backman J, Larjola J. A high efficiency microturbine concept. In: 11th European conference on turbomachinery fluid dynamics & thermodynamics ETC11. Madrid, Spain; 2015.
- [65] Xiao G, Yang T, Liu H, Ni D, Ferrari ML, Li M, et al. Recuperators for micro gas turbines: A review. *Appl Energy* 2017;197(C):83–99. <http://dx.doi.org/10.1016/j.apenergy.2017.0>.
- [66] Montero Carrero M, De Paepe W, Magnusson J, Parente A, Bram S, Contino F. Experimental characterisation of a micro humid air turbine: assessment of the thermodynamic performance. *Appl Therm Eng* 2017;118:796–806.
- [67] Balli O, Aras H. Energetic and exergetic performance evaluation of a combined heat and power system with the micro gas turbine (MGTCHP). *Int J Energy Res* 2007;31(14):1425–40. <http://dx.doi.org/10.1002/er.1308>, URL <https://onlinelibrary.wiley.com/doi/abs/10.1002/er.1308>. eprint: <https://onlinelibrary.wiley.com/doi/pdf/10.1002/er.1308>.
- [68] De Paepe W, Delattin F, Bram S, Ruyck JD. Water injection in a micro gas turbine - assessment of the performance using a black box method. *Appl Energy* 2013;112:1291–302.
- [69] Cumpsty NA. Compressor Aerodynamics. 2nd ed. Malabar, Florida: Krieger Publishing Company; 2004.
- [70] Walsh PP, Fletcher P. Gas turbine performance, 2nd ed., [repr.]. Oxford: Blackwell Science; 2008.
- [71] De Paepe W, Coppitters D, Abraham S, Tsirikoglou P, Ghorbaniasl G, Contino F. Robust operational optimization of a typical micro gas turbine. In: *Energy Procedia. Innovative solutions for energy transitions*, vol. 158, 2019, p. 5795–803. <http://dx.doi.org/10.1016/j.egypro.2019.01.549>, URL <https://www.sciencedirect.com/science/article/pii/S1876610219305739>.
- [72] Pappa A, Briceux L, Bénard P, De Paepe W. Can water dilution avoid flashback on a hydrogen-enriched micro-gas turbine combustion—A large eddy simulations study. *ASME J Eng Gas Turbines Power* 2021;143(4):041008.
- [73] Hermann F, Klingmann J, Gabrielson R. Computational and experimental investigation of emissions in a highly humidified premixed flame. In: ASME conference proceedings. 2003, p. 819–27.
- [74] Rao AD. Process for producing power. (US4829763A). 1989, URL <https://patents.google.com/patent/US4829763A/en>.
- [75] Calabria R, Chiariello F, Massoli P, Reale F. CFD analysis of turbec t100 combustor at part load by varying fuels. In: Turbo expo: power for land, sea, and air. 2015, Volume 8: Microturbines, Turbochargers and Small Turbomachines; Steam Turbines.
- [76] Takeishi K, Krewinkel R. Advanced gas turbine cooling for the carbon-neutral era. *Int J Turbomach Propuls Power* 2023;8(3). <http://dx.doi.org/10.3390/ijtp8030019>, URL <https://www.mdpi.com/2504-186X/8/3/19>.
- [77] De Paepe W, Pappa A, Montero Carrero M, Briceux L, Contino F. Reducing waste heat to the minimum: Thermodynamic assessment of the M-power cycle concept applied to micro gas turbines. *Appl Energy* 2020;279:115898. <http://dx.doi.org/10.1016/j.apenergy.2020.115898>, URL <https://www.sciencedirect.com/science/article/pii/S0306261920313647>.
- [78] De Paepe W, Pappa A, Coppitters D, Montero Carrero M, Tsirikoglou P, Contino F. Recuperator performance assessment in humidified micro gas turbine applications using experimental data extended with preliminary support vector regression model analysis. *J Eng Gas Turbines Power* 2021;143(071030). <http://dx.doi.org/10.1115/1.4049266>.
- [79] Montero Carrero M, Sánchez I, De Paepe W, Parente A, Contino F. Is there a future for small-scale cogeneration in europe? Economic and policy analysis of the internal humid air turbine cycles. *Energies* 2019;12(3):1–27, Publisher: MDPI.